AAVrh.10-Mediated APOE2 Central Nervous System Gene Therapy for APOE4-Associated Alzheimer's Disease

Jonathan B. Rosenberg,[1] Michael G. Kaplitt,[2] Bishnu P. De,[1] Alvin Chen,[1] Thomas Flagiello,[1] Christiana Salami,[1] Eduard Pey,[1] Lingzhi Zhao,[3] Rodolfo J. Ricart Arbona,[4] Sebastien Monette,[5] Jonathan P. Dyke,[6] Douglas J. Ballon,[1,6] Stephen M. Kaminsky,[1] Dolan Sondhi,[1] Gregory A. Petsko,[3] Steven M. Paul,[7] and Ronald G. Crystal[1,*]

Departments of [1]Genetic Medicine and [2]Neurosurgery, [3]Appel Alzheimer's Disease Research Institute, Feil Family Brain and Mind Research Institute, and [6]Department of Radiology, Weill Cornell Medical College, New York, New York; [4]Center of Comparative Medicine and Pathology, Memorial Sloan Kettering Cancer Center, New York, New York; [5]Laboratory of Comparative Pathology, Memorial Sloan Kettering Cancer Center, The Rockefeller University, Weill Cornell Medical College, New York, New York; and [7]Voyager Therapeutics, Inc., Cambridge, Massachusetts.

Alzheimer's disease (AD) is a progressive degenerative neurological disorder affecting nearly one in nine elderly people in the United States. Population studies have shown that an inheritance of the apolipoprotein E (APOE) variant *APOE4* allele increases the risk of developing AD, whereas *APOE2* homozygotes are protected from late-onset AD. It was hypothesized that expression of the "protective" APOE2 variant by genetic modification of the central nervous system (CNS) of APOE4 homozygotes could reverse or prevent progressive neurologic damage. To assess the CNS distribution and safety of APOE2 gene therapy for AD in a large-animal model, intraparenchymal, intracisternal, and intraventricular routes of delivery to the CNS of nonhuman primates of AAVrh.10hAPOE2-HA, an AAVrh.10 serotype coding for an HA-tagged human APOE2 cDNA sequence, were evaluated. To evaluate the route of delivery that achieves the widest extent of APOE2 expression in the CNS, the expression of APOE2 in the CNS was evaluated 2 months following vector administration for APOE2 DNA, mRNA, and protein. Finally, using conventional toxicology assays, the safety of the best route of delivery was assessed. The data demonstrated that while all three routes are capable of mediating ApoE2 expression in AD relevant regions, intracisternal delivery of AAVrh.10hAPOE2-HA safely mediated wide distribution of ApoE2 with the least invasive surgical intervention, thus providing the optimal strategy to deliver vector-mediated human APOE2 to the CNS.

Keywords: Alzheimer's disease, APOE2, AAV, gene therapy, CNS

INTRODUCTION

Alzheimer's disease (AD), a progressive neurodegenerative disorder, currently affects more than five million people in the United States and is rapidly increasing in prevalence and economic impact.[1,2] By 2050, one new case of AD is expected to develop every 33 s, or nearly a million new cases per year, with a total estimated prevalence of 13.8 million. AD is the sixth leading cause of death in the United States and the fifth leading cause of death in individuals ≥65 years.[2] Currently approved drugs do little to limit disease progression, and no preventive therapies are available.[3,4]

The major risk factor for AD is inheritance of the *E4* allele of apolipoprotein E (APOE).[5,6] There are three common *APOE* alleles (E2, E3, and E4), each encoding APOE isoforms expressed primarily in the liver and brain.[7,8] *APOE4* homozygotes have a markedly increased risk of developing AD (14.5-fold compared to *APOE3* homozygotes), as well as an earlier age of onset for developing the disease (approximately 5 years for each *APOE4* allele compared to *APOE3* homozygotes).[6,9,10] Between 45% and 50% of AD patients carry at least one *APOE4* allele compared to only 15% of age-matched healthy controls.[5,11] In contrast, APOE2 is a protective

*Correspondence: Dr. Ronald G. Crystal, Department of Genetic Medicine, Weill Cornell Medical College, 1300 York Avenue, Box 164, New York, NY 10065. E-mail: geneticmedicine@med.cornell.edu

DOI: 10.1089/humc.2017.231

allele, reducing AD risk by approximately 50% (1.8-fold decreased risk) and markedly delaying the age of onset, even in the presence of the *APOE4* allele.[12,13] In humans, the *APOE4* and *APOE2* alleles are codominant; *E2/E4* heterozygotes have only double the risk of *E3/E3* homozygotes, and equivalent expression of E2 almost cancels out the deleterious effect of the *E4* allele.[6,14,15]

There is strong experimental evidence that the APOE isoforms are major determinants of the amount and quality of amyloid-β peptide (Aβ) and amyloid burden in the brain that develops during aging.[15–17] Crossing a transgenic mouse model of AD that has high levels of human Aβ in the brain with human *APOE* targeted replacement mice demonstrated age-dependent and APOE isoform-dependent (E4>>E3>E2) Aβ deposition and amyloid burden in the brain in a manner that recapitulates the human condition observed in pre-symptomatic elderly *APOE4* carriers as well as AD patients.[18–21]

Based on these observations, one strategy to prevent AD in *APOE4* carriers is to modify the central nervous system (CNS) genetically to express APOE2, providing the CNS with the protective APOE2 to balance the AD risk associated with expression of APOE4.[22–26] Studies with a lentiviral vector expressing APOE2 delivered directly to the hippocampus of a transgenic AD mouse established a robust protective effect of the *APOE2* allele on AD risk, with an observed rapid, significant reduction in brain amyloid burden and neuritic plaques.[23] The protective effect of *APOE2* genetic modification of the CNS was replicated by Hudry *et al*.[24] using an adeno-associated virus serotype 4 (AAV4) vector to deliver APOE2 into the cerebrospinal fluid (CSF) of the lateral ventricle of mice overexpressing a mutant β-amyloid precursor protein (APP) transgene and by the Paul and Crystal laboratories[26] demonstrating APOE2-mediated efficacy in an AD *E4* transgenic (APP.PS1.TRE4) mouse model with an AAVrh.10 vector encoding the human *APOE2* cDNA (AAVrh.10hAPOE2).

As the next step in moving APOE2 gene therapy for AD to the clinic, the focus of the present study was to determine the most effective safe route of the AAVrh.10 vector delivery to mediate widespread distribution of therapeutic levels of the *APOE2* gene, mRNA, and protein in the CNS of nonhuman primates (NHP). AAVrh.10hAPOE2-HA, an rh.10 serotype of AAV coding for an HA-tagged human *APOE2* cDNA sequence, was administered to the CNS of African Green NHP by three different routes: (1) direct intraparenchymal to three sites in the hippocampal region; (2) intracisternal to the cisterna magna; and (3) intraventricular to the frontal horn of the third ventricle. NHPs were evaluated for *APOE2* DNA, mRNA, and protein in CSF over time and in CNS tissue at 2 months following therapy in order to determine the route and/or site of infusion that achieves the widest spread and persistence of APOE2 expression. Finally, using conventional toxicology assays, the safety of the three routes of delivery was assessed. The data demonstrated that while all three routes are capable of mediating APOE2 expression in AD relevant regions, intracisternal delivery of an AAVrh.10 vector coding for *APOE2* provides widely distributed APOE2 and is the least invasive, providing a safe way to deliver vector-mediated hAPOE2 to the CNS.

METHODS

Gene transfer vector

The AAVrh.10hAPOE2-HA vector was produced under current Good Manufacturing Practice conditions at the Belfer Gene Therapy Core Facility, Department of Genetic Medicine, Weill Cornell Medical College, by co-transfection of two plasmids: one coding for the therapeutic gene (pAAV2-CAG-hAPOE2-HA), and the other providing AAV replication and capsid functions plus the adenoviral helper functions (pPAK-MArh.10) into a stable human embryonic kidney cell line (293T) in the presence of PEI reagent (Polysciences, Warrington, PA). The pAAV2-CAG-hAPOE2-HA plasmid is comprised of an AAV2 gene transfer vector backbone (the inverted terminal repeats [ITRs] of AAV2 flanking the expression cassette) and an expression cassette with a human cytomegalovirus enhancer/promoter and the splice donor and the left-hand intron sequence from chicken β-actin/right-hand intron sequence and splice acceptor from rabbit β-globin (this enhancer/promoter/intron sequence is referred to as "CAG"), the full-length human *APOE2* cDNA and an optimized Kozak translational initiation signal prior to the start codon, hemagglutinin (HA) peptide fused to the 3′ end of *APOE2* cDNA, and a rabbit β-globin poly A sequence[27–29] (Fig. 1). The CAG promoter in the AAVrh.10hAPOE2 vector was chosen because it is a strong ubiquitous promoter, successfully used to drive gene expression in AAV vectors in the CNS on a persistent basis.[27–34] In order to differentiate vector-mediated expression of *APOE2* transgene and protein over the endogenous *APOE2* in the NHP brain, the human *APOE2* was HA-tagged on the 3′ terminus. The pooled cell harvest (centrifuged at 1,150 *g* for 15 min at 4°C) was subjected to

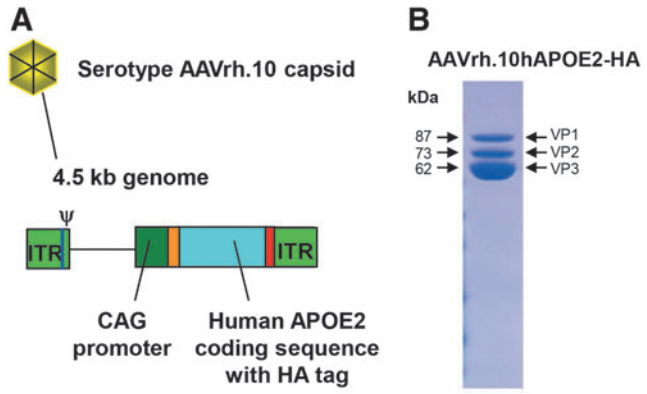

Figure 1. AAVrh.10hAPOE2-HA vector. **(A)** Schematic. The vector is comprised of the AAVrh.10 serotype capsid, and the genome is comprised of the adeno-associated virus (AAV) serotype 2 inverted terminal repeats (ITR), encapsidation signal (Ψ), and the expression cassette, including the CAG promoter (the human cytomegalovirus [CMV] enhancer; chicken β-actin promoter/splice donor and 5′ end of intron; 3′ end of the rabbit β-globin intron and splice acceptor), the normal human *APOE2* cDNA with an hemagglutinin (HA) epitope sequence tag at the 3′ end, and the polyadenylation/transcription stop signal from rabbit β-globin. **(B)** Sodium dodecylsulfate polyacrylamide gel electrophoresis of AAVrh.10hAPOE2. The VP1–3 bands associated with the AAV vector capsid proteins align with the expected molecular weights.

multiple freeze/thaw cycles to release the AAVrh.10hAPOE2-HA from the cells, producing CVL. Digestion of any extra viral DNA was carried out using a recombinant human DNase (Benzonase, 50 IU/mL; Sigma–Aldrich, St. Louis, MO) in the presence of $MgCl_2$ (25 mM Tris-HCl, pH 7.5, 0.14 M NaCl, 5 mM KCl, 0.7 mM K_2HPO_4, 15 mM MgCl $\cdot 6H_2O$ buffer) on thawed CVL and then centrifuged at 3,300 *g* for 20 min. The resulting vector was purified by differential density using an iodixanol gradient. The pooled iodixanol fractions were diluted 3.5:1 in Binding Buffer (0.05 M Tris, pH 9.0, 0.05 M NaCl), and applied to a 5.0 mL HiTrap QHP column (GE Healthcare, Piscataway, NJ). The column was washed twice in binding buffer and then buffer exchanged in 1×phosphate-buffered saline (PBS), pH 7.4. The final solution was concentrated in Amicon Ultra-15 100 KDa centrifugal concentrator (Millipore, Darmstadt, Germany), then sterile filtered through a 0.22 μm membrane filter, dispensed at prescribed volumes into cryovials, and frozen at –80°C until administration on the day of surgery. Vector titer was determined by real-time polymerase chain reaction (PCR; TaqMan) with absolute quantitation. To confirm vector function, supernatant from AAVrh.10hAPOE2-HA infected 293-ORF6 cells was assayed for expression of ApoE2 by Western blot analysis. Samples of the CVL were taken for quality control assays that evaluated the presence of adventitious agents. The final purified product was characterized with assays for measures of identity, potency, and purity.

Recombinant AAVrh.10Luc vector used for *in vitro* assays was produced following the same protocol as described above for AAVrh.10hAPOE2-HA, but using a luciferase vector plasmid (same as pAAV2-CAG-hAPOE2-HA but with the *APOE2-HA* transgene replaced by a firefly luciferase gene), and the AAVrh.10 packaging plasmid (pPAK-MArh.10) for transfection. The AAVrh.10Luc vector was propagated, purified, and stored as described above.

AAVrh.10hAPOE2-HA and AAVrh.10Luc vectors were titered for genome copies by quantitative PCR using TaqMan-based analysis reagents (Applied Biosystems, Foster City, CA) and a CAG-specific primer–probe set to amplify the vector promoter region (forward primer: GTCAATGGG TGGAGTATTTACGG; reverse primer: AGGTCAT GTACTGGGCATAATGC), designed using Primer Express software (Applied Biosystems). Prior to PCR analysis, the isolated AAVrh.10 vectors were digested with Proteinase K in a 0.5% sodium dodecyl sulfate (SDS) and 25 mM ethylenediaminetetraacetate (EDTA) buffer at 55°C for 1 h, followed by denaturing of Proteinase K at 95°C for 15 min. To generate a standard curve, an AAV-CAG-hCLN2 plasmid, with a known copy number, was prepared fresh using serial dilutions from 1×10^8 to 10 copies/μL for each AAVrh.10 preparation, as previously described.[29] All samples were run in triplicate (standard curve plasmids, QC DNA samples, test samples [unknown], and positive and negative controls), using the QuantStudio 6 Flex System with SAE (Security, Audit, and Electronic Signature) Module. The PCR reactions were performed using the QuantStudio6 Flex system (Applied Biosystems) at 50°C for 2 min; 95°C for 10 min; 40 cycles of 95°C for 15 s, and 60°C for 60 s. Acceptance criteria for the assay include specifications for the correlation coefficient (R^2) of the standard curve, the reaction efficiency as measured by the slope of the standard curve, and the positive and negative controls. For the QC DNA samples, the copy numbers should have a percent relative error (RE) of <20% with a replicate Ct CV of ≤2%.

NHPs

Adult *Chlorocebus aethiops sabaeus* NHPs (4- to 7-year-old male African Green monkeys; weight 5–8 kg) were purchased from World Wide Primates (Miami, FL). All NHPs used were quarantined for a 3-month period after arrival and were deemed in good health and suitable for experimental use. None of the animals had previously been used for

any other experiments. NHPs were maintained in paired-housed cages, fed twice daily with monkey chow (monkey diet jumbo; PMI Nutrition International, Brentwood, MO), and supplemented with fruit or vegetables daily, with access to water *ad libitum*. All experiments were conducted in an AAALAC-accredited facility and approved by the Institutional Animal Care and Use Committee of Weill Cornell Medical College (New York, NY).

Presurgical magnetic resonance imaging and coordinate mapping

All imaging was performed at the Citigroup Biomedical Imaging Center (CBIC), Weill Cornell Medical College. To determine the precise location of burr hole placement and angle/depth of the catheter tip necessary for targeting the intracranial regions with vector administration, each NHP underwent magnetic resonance imaging (MRI) and computerized axial tomography (CAT) of the brain prior to surgery. NHPs were anesthetized with ketamine (5–10 mg/kg) plus dexmedetomidine (0.015–0.02 mg/kg) given intramuscularly (i.m., quadriceps), endotracheally intubated, and maintained on gas anesthesia (isoflurane) during the procedure, and provided with fluids through a catheter inserted into a saphenous vein. The head was mounted in a MRI-compatible stereotaxic frame (David Kopf Instruments, Tujunga, CA) using ear bars, a palate clamp, and ventral orbit clamps. An 11 cm diameter loop coil was placed on top of the NHP and frame in an MRI scanner used for human imaging (Magnetom Trio, 3.0 Tesla; Siemens Healthcare, Malvern, PA). T1 and T2 weighted scans were acquired, and the NHP was removed from the scanner and transferred while still attached to the head frame to a computed tomography (CT) scanner (Biograph mCT; Siemens Healthcare) to generate a combined image of the brain and the stereotactic frame in order to guide the placement of catheters accurately. The MRI and CT images were fused to generate a three-dimensional (3D) map of the brain from which the stereotaxic coordinates were determined using Brainlab iPlan Stereotaxy 3.0 software (Westchester, IL) to align the delivery arms over the skull and provide the correct angle and depth needed to reach the designated targets in the brain parenchyma. For safety assessments, three NHPs (NHP-10, –11, and –12) were imaged prior to surgery and at 8 weeks post administration of the vector administered by both the intracisternal and intraventricular routes, and compared to brain scans of a non-treated NHP (NHP-13).

Vector administration

All routes of vector administration involved the same pre- and post-operation procedures. The NHPs were fasted for >16 h prior to the procedure. Prior to the sedation, each NHP was videotaped for pre-surgery (day 0) behavior safety assessments. The animals were anesthetized with an i.m. injection of ketamine (5–10 mg/kg) plus dexmedetomidine (0.015–0.02 mg/kg) in the medial thigh muscle, followed by inhaled isoflurane (1–3%). Intravenous fluids (Lactated Ringers' solution) were provided throughout each procedure lasting >20 min. Vital signs were recorded, and blood was drawn for baseline blood and serum chemistry parameters, as well as for determining anti-AAV titers. NHPs received standard postoperative veterinary care. The NHPs were carefully laid back in their home cage in the recovery position (the left side) and closely monitored while recovering from anesthesia. A neurological exam was given following full recovery from sedation, assessing paralysis by monitoring the NHP's muscle movements on both sides, use of all extremities for climbing, facial muscle usage (yawning, chewing), eye reactivity, and ability to stand from recovery position (on left side). The NHPs were assessed three times a day during recovery from surgery over the first 72 h by trained animal technicians and daily thereafter. For additional safety assessment, the NHP behavior was filmed at 1, 2, 4, and 8 weeks after surgery for blinded assessment of normal and abnormal behaviors.

Intraparenchymal (intrahippocampal) administration route (n = 2). For this route, vector was administered via a surgical procedure into the brain parenchyma to target the hippocampal region directly in the lower temporal lobes (Supplementary Fig. S1A; Supplementary Data are available online at www.liebertpub.com/humc). Each animal was anesthetized, as described previously. The animals were positioned in a Kopf stereotaxic frame with bilateral ear bars in the same position as recorded from the MRI session. The scalp was shaved with an electric razor, and the area was prepped and draped in sterile fashion. Bupivacaine (0.25% solution) was injected subdermal at the intended midline incision site 5 min before the skin and cranial aponeurosis were incised with a #10 scalpel blade. Tissues were retracted laterally to expose the craniotomy sites on the calvarium. Sterilized manipulators were attached to stereotaxic frame and burr hole sites marked using a sterile marking pen at predetermined coordinates obtained from the MRI/CT scan. Anterior/posterior (A/P)

measurements were from the ear bar set at 0. 0 mm. Midline (M/L) measurements were from the central coronal suture. Burr holes were made corresponding to the predetermined tract for administration sites using a sterile 3 mm drill bit. To guide the micro-catheters into the cortex, 22G 3.5″ Quincke spinal needles (Becton Dickinson, Franklin Lakes, NJ) were clamped to each stereotaxic arm. A microcapillary catheter (previously described[31]) was then threaded down the spinal needles to predetermined depth coordinates. The targets were calculated by setting the visualized pia dural measurement as 0 mm. All stereotaxic arms were set at 0°, unless noted. Each NHP had two catheters threaded down to the targeted region, one per hemisphere, with multiple release targets along the dorsal–ventral trajectory in the hippocampus and entorhinal cortex. One trajectory was inserted at an angle to inject the entorhinal cortex directly, while the other trajectory in contralateral hemisphere followed the dorsal–ventral axis. The right hemisphere catheter stereotactic coordinates were: +1.2 cm anterior (A/P); 1.35 cm lateral from midline (M/L); with manipulator arm angled at 9° from vertical. Vector deposit #1 was at 3.4 cm, #2 at 3.1 cm, and #3 at 2. 7 cm from the pia mater. The left hemisphere catheter stereotactic coordinates were: +1.2 cm anterior (A/P); 1.30 cm lateral from midline (M/L); with manipulator arm straight (0° from vertical). Vector deposit #1 was at 3.5 cm, #2 at 3.2 cm, and #3 at 2.8 cm from the pia mater. The total dose of vector was the same for both animals: 5×10^{12} genome copies (gc; $0.7–1.2\times10^{12}$ gc/kg) of AAVrh. 10hAPOE2-HA, administered intracerebrally to six sites in the hippocampal region, bilaterally, with three sites per hemisphere along one catheter tract, 15 μL per injection site (infusion rate of 1 μL/min). After completion of the vector administrations at each burr hole site, the catheter needle was slowly removed. Galea muscles were closed with 3-0 Vicryl followed by a 4-0 resorbable subcuticular layer. The NHP was then removed from the stereotaxic frame and placed in the recovery position until awake. Postoperative analgesia was carprofen (4.0 mg/kg, subcutaneously [s.c.]) and buprenorphine (0.05 mg/kg) given i.m. during the anesthetic recovery period.

Intracerebral ventricular administration route (n = 3). Vector was administered directly into the cerebral-ventricular system via one unilateral burr hole into the left or right frontal ventricle (Supplementary Fig. S1A). Anesthetized NHPs were placed back into the Kopf stereotactic frame, and the head placement was adjusted to match the previous MRI coordinates. For this route, a single burr hole and catheter insertion was used to deliver the vector to either the left or right hemisphere. An incision ~6 cm perpendicular to the midline was made to expose the central suture and the target location in the left or right frontal lobe. A stereotactic manipulator arm clamp was set up with a sterile 22G 1.0″ needle (Becton Dickinson) for skull target marking and for penetration into the ventricle. The angle of the manipulator was set at 20–25°. The target site (frontal horn of lateral ventricle) was calculated using a manipulator arm gauge, for example the ventricular administration site was at 22.9 mm A/P, superior in aspect to the ear bars (at 0 A/P, 0 D/V), +9.2 mm M/L, using an angle of 24.9°, and 18.7 mm depth along the angle using the top of the pia. Upon reaching the target depth, pulsating CSF was observed in the base of the needle hub, and CSF was collected (~250 μL) for analysis. Vector (1.0–1.3 mL; 5×10^{13} gc) was then infused in a sterile fashion over 6 min (200 μL/min) as a single bolus. Next, the manipulator arm and needle were slowly withdrawn through the brain parenchyma, and the hole was checked for reflux once the needle was out of the skull. The incision was closed using sutures (Vicryl 2-0 polyglactin absorbable first for muscle, interrupted sutures; 3-0 Ethilon nylon for outer skin, non-interrupted). At the completion of the surgery, the NHP was removed from head frame and placed in left-side recovery position. Anesthesia recovery and postoperative procedures were conducted, as previously described.

Intracisternal administration route (n = 3). For this route, the vector was administered to the cisterna magna at the posterior of the skull via a nonsurgical method (Supplementary Fig. S1A). The animals were sedated with ketamine (5–7 mg/kg) and dexmedetomidine (0.015–0.02 mg/kg) given i.m. The dorsal upper neck/lower skull area was shaved, and the skin thoroughly scrubbed with alternating Nolvasan and 70% alcohol on the neck region. The injection site at the base of the skull was draped with sterile towels, leaving the injection site exposed. The NHPs were placed on right side, and the hind limb reflexes were checked to make sure the animal was free and relaxed. The head was then held bent forward, in the lateral decubitus position, and occiput projections were found by palpation. A sterile 22G 1.5″ spinal needle (Becton Dickinson) was used to pierce the neck skin medially ~1 cm distal to the protuberantia occipitalis externa. The tip of the needle was then

inserted into the cisterna magna. The position of needle was confirmed by free flow of clear CSF back into the hub, with collection of $\sim 500\,\mu$L for later analysis. The CSF was examined to ensure there was no blood contamination. Vector was administered to the cisterna magna (1.0–1.3 mL, 5.0×10^{13} gc), infused over 2 min (0.5 mL/min), followed by a saline flush (0.5 mL). The spinal needle was then removed quickly with no fluid loss or blood. Direct pressure on the injection site was maintained for 3–5 min to prevent leakage of vector. After intracisternal infusion, animals were given carprofen (4 mg/kg) i.m. for analgesia and atipamezole (0.1–0.2 mg/kg) i.m. to accelerate recovery. When awake, the animals were removed from procedure room and returned to their housing.

Dual intracisternal plus intraventricular administration route (n = 3). To minimize the use of NHPs for safety assessments, vector (5×10^{13} gc/route) was administered to three NHPs via both the intracisternal and intracerebral ventricular routes. Vector was first administered via the intraventricular route followed immediately by a second infusion of vector to the cisterna magna. The NHP was prepped for surgery, as described above for the intraventricular route, and following successful delivery of vector to the frontal ventricle, the incision was sutured and the NHP was removed from the head frame, all while still anesthetized. The NHP was then placed on the left side, as described in the intracisternal route method, followed by delivery of the vector to the second site via spinal needle into the cisterna magna. The intracisternal bolus was delivered within 10 min following completion of the intraventricular delivery.

Safety assessment

The NHPs were observed and monitored daily by the experienced husbandry technicians and research specialists for general appearance, distress, and changes in behavior. The animals were housed singly following surgery but paired at all other times. Behavioral assessments were recorded with NHPs in separate cages to minimize the interference by a cohabitating NHP. At 1 week before surgery, on the day of administration, and at 1, 2, 4, and 8 weeks (±1–2 days) post surgery, animals were sedated for general health assessment and for blood sampling for complete blood count (CBC), serum chemistries, and anti-AAV total and neutralizing antibody titers. Complete blood tests were performed by the Laboratory of Comparative Pathology (LCP) with an IDEXX Procyte DX hematology analyzer, and the following parameters were measured: white cell count (WBC), red blood cell count (RBC), reticulocytes (% and absolute), hemoglobin, hematocrit, mean corpuscular volume (MCV), mean corpuscular hemoglobin (MCH), mean corpuscular hemoglobin concentration (MCHC), segmented neutrophils (% and absolute), lymphocytes (% and absolute), monocytes (% and absolute), eosinophils (% and absolute), basophils (% and absolute), and platelet count. Serum chemistry was performed by the LCP on a Beckman Coulter AU680 serum chemistry analyzer, and the following parameters were measured: alkaline phosphatase (ALP), alanine aminotransferase (ALT), aspartate aminotransferase (AST), gamma glutamyl transferase (GGT), albumin, total protein, globulin, total bilirubin, direct bilirubin, indirect bilirubin, blood urea nitrogen (BUN), creatine kinase (CK), cholesterol, triglycerides, glucose, lactate dehydrogenase (LDH), calcium, phosphorus, bicarbonate, amylase, lipase, magnesium, sodium, chloride, potassium, sodium/ potassium (Na/K), albumin/ globulin (A/G), and BUN/ creatinine (B/C) ratios, and anion gap. The values from the control animal in this study and controls in previous studies with African Green monkeys were used to calculate normal ranges (total 65 blood samples from 29 individual male NHPs) and establish the upper and lower limits of normal African Green monkey values for comparisons of pre- and post-surgery blood/serum parameters.[31,35]

Anti-AAV total antibody titers. Anti-AAVrh.10 antibody titers were measured using an enzyme-linked immunosorbent assay (ELISA). Flat bottomed 96-well enzyme immunoassay plates (Corning, New York, NY) were coated with 100 μL of 10^{10} gc/mL AAVrh.10Luc (identical to AAVrh.10hAPOE2-HA but coding for luciferase) in carbonate buffer, pH 9.4, overnight at 4°C. The wells were blocked with 5% milk in PBS for 30 min at 23°C. Sera from NHPs that had been treated with AAVrh.10hAPOE2-HA was twofold serially diluted, added to each well, and incubated for 90 min at 23°C. The plates were washed three times with PBS plus 0.05% Tween 20 (PBS-Tween). The plates were then incubated with 100 μL of 1:2,000 diluted horseradish peroxidase (HRP)-conjugated goat anti-monkey immunoglobulin G (IgG; Santa Cruz Biotechnology, San Diego, CA) in 1% milk in PBS for 90 min at 23°C. The plates were washed three times with PBS-Tween followed by once with PBS. Peroxidase substrate (BioRad, Hercules, CA), 100 μL/well, was added and incubated in the dark for 20 min at 23°C, and the reaction was stopped by adding 2% oxalic acid (100 μL/well). Absorbance was measured at 415 nm. Anti-AAVrh.10

antibody titers were calculated by interpolation of the log(OD) versus –log(dilution), with a cutoff value equal to twofold the absorbance of background.

Anti-AAV neutralizing titers. AAVrh.10 neutralizing antibody titers were assessed at various times using an *in vitro* assay with 293-ORF6 cells in 96-well plates using AAVrh.10Luc. AAVrh.10Luc was incubated with serial dilutions of NHP sera at 37°C for 45 min and then used to infect cells at a multiplicity of infection of 3,000 gc/cell. At 48 h post infection, luciferase activity was assessed with the Luciferase Assay System (Promega, Madison, WI). The neutralizing antibody titer was expressed as the reciprocal of serum dilution at which 50% inhibition of AAVrh.10Luc was observed.[36]

Behavioral assessments. At five time points (pre, 0, 1, 4, and 8 weeks post surgery, ±1–2 days), prior to sedation for blood draws, all NHPs were assessed for behavioral changes by videotaping. Each NHP was separated in individual home cages in the absence of stimuli and then challenged with specific food/threat scenarios. Each NHP was videotaped for 3 min in the absence of outside stimuli to observe non-stimulated "normal" behavioral activity, and then for another 2 min to gauge their response to positive (food treats) and negative (threatening stares) reinforcements. Behaviors were scored by observers ($n=2$) blinded to treatment and route from the videotape sessions for number of times the NHPs performed specific normal ($n=14$) and abnormal ($n=6$) behaviors, scoring "1" for 5 s of each behavior. The sum of normal behaviors (anxiety, arousal, and quiet behaviors) was calculated as the "healthy" score (defined in Supplementary Table S1). The sum of abnormal behaviors (sedation and abnormal motions) was calculated as the "abnormal" score for each session (defined in Supplementary Table S1). Additional assessments were made to rate the NHPs' response to food and threats for delayed responses over a 1 min period (0 = normal and 5 = abnormal). The NHP behaviors were compared to an extensive data set.[31,35]

Necropsy and sample collection

All NHPs were euthanized 8 weeks post administration (day 56 ± 2 days). Prior to euthanasia, safety assessments were performed on all NHPs (behavior, weight, blood, and CSF sampling), as described above. The dual-route and sham animals had additional testing performed for safety aspects of the study, including CNS MRI scans at 8 weeks. At sacrifice, euthanasia was carried out with intravenous pentobarbital until loss of corneal reflexes was achieved. Cold 1 × PBS perfusion (4 L) was performed via the cardiac left ventricle following the administration of 1,000–2,000 IU heparin. Sections of organs were collected at necropsy and fixed with 10% neutral-buffered formalin for immunohistochemistry (IHC); additional sections were flash-frozen in liquid nitrogen and stored frozen (unfixed) for later assays if required. The brain was excised, weighed, and divided into two hemispheres. The right hemisphere was processed by sectioning into 1 cm coronal slabs (seven to nine slices) and then subdividing the slabs into 1 cm^3 cubes for DNA, mRNA, and protein isolation for assessment of *APOE2* vector genome and mRNA levels by quantitative TaqMan PCR analysis, and ApoE2-HA protein levels by ELISA. The left brain hemisphere was fixed in 10% neutral-buffered formalin and sectioned into 3 mm coronal sections for assessment of the distribution of ApoE2 protein by IHC for the HA tag. The spinal cord at three levels was extracted from each NHP: cervical C3–C4, thoracic T6–T7, and lumbar L2–L4. Two samples of spinal tissue were collected at each location: one sample placed in 10% neutral-buffered formalin for histopathology (hematoxylin and eosin [H&E] and IHC stains); and the other sample partitioned as for the brain cubes and reserved for future quantitative PCR TaqMan analysis. All organs were examined grossly during necropsy performed by a board-certified veterinary pathologist, and gross findings were recorded. Samples of brain and spinal cord from all animals were fixed in 10% neutral-buffered formalin for immunohistochemical staining. In addition, for NHP-10–NHP-14, other organs detailed below were fixed in 10% neutral-buffered formalin, processed, embedded in paraffin, section at a thickness of 5 μm, stained with H&E, and examined by a board-certified veterinary pathologist, and histopathologic changes were recorded. These organs included the lungs, heart, aorta, thymus, parotid and submandibular salivary glands, biceps femoris muscle, kidneys, liver, gallbladder, stomach, duodenum, jejunum, ileum, cecum, colon, rectum, pancreas, mesenteric, tracheobronchial, popliteal, inguinal lymph node, thyroid gland, spleen, urinary bladder, adrenal, pituitary, sciatic nerve, skin, esophagus, trachea, facial nerve, glossopharyngeal nerve, pericardium, diaphragm, sternum, bone marrow, eye, optic nerve, lacrimal gland, testes, epididymis, prostate, and seminal vesicles. Samples of a subset of organs (liver, heart, lung, kidney, spleen, ileum, and any other organs with gross abnormalities discovered during the examination) were frozen unfixed for

future vector studies if necessary. All slides were evaluated by a board-certified pathologist, and observations were recorded.

Processing and quantitative analysis of CNS and spinal cord samples

During necropsy, the right hemisphere of the NHP brain was processed into 1 cm^3 cubes for vector DNA, transgene mRNA, and ApoE2-HA protein assays. The brains were sub-sectioned into ~1 cm coronal slabs with 5-inch single-edge straight blades. Slab numbering was S1–S8, with S1 = anterior frontal lobes and S8 = posterior portion of the brain (Supplementary Fig. S1B). Coronal slabs containing the site of administration, identified by cortical depressions, were labeled as the target site to help identify vector deposit loci. The slabs from the right hemisphere were further sectioned into square sections based on a predesigned 10 mm × 10 mm grid using fresh straight blades. Brain cubes (70–90 cubes, 100–450 mg) were labeled with identifiers of slab section # (S1, etc.) plus grid coordinates (A1 … C6) to allow for recreation of the 3D map of the brain (Supplementary Fig. S1B). Brain cubes were put inside labeled tubes and placed on ice. All cubes were cut into at least four sections (≤ 100 mg/piece) with a sterile #15 scalpel (Bard-Parker) and weighed. For each brain cube, one divided piece was frozen on dry ice and transferred to a –80°C freezer for later processing for protein analysis. All other pieces were reserved for DNA/mRNA isolation and transferred to a labeled clean 15 mL conical tube, with 1 mL of RNAlater (Qiagen, Germantown, MD) per 100 mg brain sample. DNA/mRNA samples were incubated at 4°C overnight to allow for stabilization of mRNA by RNAlater. After 24–72 h, the samples were retrieved from the RNAlater solution for homogenization. Brain samples were homogenized using Qiagen's Buffer RLT with β-mercaptoethanol (600 μL per 30 mg tissue weight) with two 5 mm stainless steel beads (Qiagen), using the TissueLyser LT (Qiagen) at 4°C for 10–20 min at 50 Hz. Homogenized tissue was collected, and a uniform 300 μL sample was removed for DNA with a separate 300 μL aliquot for mRNA processing, with the remainder frozen at –80°C in reserve.

DNA isolation. For tissue homogenates processed for DNA, the DNeasy Blood and Tissue Kit (cat #69506; Qiagen) was used. Approximately 50 mg of homogenized tissue sample was digested with a digest mix containing 10 μL Proteinase K and 140 μL sterile water at 56°C for 10 min. Next, RNase digestion was performed, where 4 μL of 100 mg/mL RNase A was added to the homogenized tissue, followed by vortexing and incubation at room temperature for 2 min. This was followed by centrifugation at 13,000 *g* for 3 min, after which the supernatant was transferred to a tube containing 225 μL ethanol (96–100%) and loaded onto a DNeasy mini spin column. After a series of centrifugation steps with the Qiagen kit buffers AW1 and AW2 at >6,000 *g* at room temperature in an Eppendorf 5424 centrifuge, the DNA was eluted using 100 μL Buffer AE and saved as 1 × 20 μL and 1 × 80 μL aliquots at –20°C for analysis.

RNA isolation. For tissue homogenates processed for mRNA, the RNeasy Lipid Tissue Mini kit (Qiagen) was used. Approximately 50 mg (~300 μL) of homogenized tissue sample was digested with 500 μL QIAzol lysis reagent from kit at 23°C for 5 min, followed by the addition of 200 μL chloroform and mixing vigorously for 15 s, and incubation at 23°C for 3 min. The mixture was then centrifuged at 12,000 *g* for 15 min at 4°C. The aqueous phase was transferred to a tube containing 300 μL ethanol (70%), vortexed, loaded onto an RNeasy Mini spin column, and centrifuged for 15 s at ≥8,000 *g* at 23°C. Buffer RW1 (350 μL) was then added to the RNeasy Mini column, vortexed, and centrifuged for 15 s at ≥8,000 *g* at 23°C. DNase digestion performed using DNase I (80 μL) mix (10 μL DNase I and 70 μL buffer RDD) added to the RNeasy mini spin column, and incubating for 15 min at 23°C. After a series of wash steps with buffers RW1 and RPE and centrifugation at ≥8,000 *g*, the RNA was eluted using 30 μL RNAsecure (RNase-free water), and centrifugation at ≥8,000 *g* for 1 min at 23°C. RNA was saved at –80°C for future analysis. A 5 μL aliquot was reserved for RNA quality analysis (RIN) and nanodropped to determine total RNA concentration.

Protein isolation. To measure human ApoE2-HA protein, brain cubes were homogenized in 300 μL lysis buffer (10 mM HEPES-KOH, pH 7.4, 5 mM mannitol, and 1% Triton X-100 in water) using 5 mm stainless steel beads in a TissueLyzer LT (Qiagen, Valencia, CA) for 2 × 10 min at oscillation of 50/s. The homogenates were centrifuged at 10,000 *g* for 5 min in an Eppendorf centrifuge. Supernatants were collected and stored in aliquots at –80°C until use.

DNA, mRNA, and protein analysis

AAVrh.10hAPOE2-HA vector genome copies in the CNS brain cubes were measured by PCR using a TaqMan-based analysis (Applied Biosystems

"Universal Master Mix II, no UNG" reagent) and a human-specific primer/probe set (Applied Biosystems) to detect the 3′ terminus of the human *APOE2* cDNA (including the HA-tag sequence) from viral genomes, in the background of primate genomic DNA (forward primer: 5′-GTGGAGAAGG TGCAGGCT-3′; reverse primer: 5′-AAGCGTAATC TGGAACATCGT-3′; probe, 5′-CCCTGTGCCCAGC GACAATC-3′). The PCR was performed using the QuantStudio6 Flex system (Applied Biosystems) at 50°C for 2 min and 95°C for 15 min; 40 cycles of 95°C for 15 s and 60°C for 60 s, with a rate of $\Delta = 1.6$°C/s, and the results expressed as vector genome copy number per μg DNA. Each sample was analyzed in duplicate. Samples that failed amplification were re-extracted and retested. Samples were scored as positive for vector genome if the *APOE2* sequence Ct value was <35, and were scored vector negative if transgene sequence Ct value was >36. All assays were performed with a standard curve based on a hAPOE2-HA plasmid (10^8–10^1 gc) run in triplicate. The resulting copy numbers were used for 3D recreations by coloring each cube based on predetermined cutoff values to model volumes of distribution in the brain.

mRNA expressed from the vector transgene was quantitatively measured in parallel to the genomic samples. For the mRNA TaqMan assays, the mRNA was first converted to cDNA using random hexamers and reverse transcriptase using one cycle of 25°C for 10 min, 42°C for 60 min, and 95°C for 5 min, and then held at 4°C, using the GeneAmp PCR System 9700 machine (Applied Biosystems). The samples were amplified by using the same PCR conditions and standard plasmid curve as described above, with the results expressed as transgene mRNA number per μg cDNA.

Human ApoE2-HA protein was quantified in AAVrh.10hAPOE2-HA administered brain homogenates and CSF samples using a mouse anti-HA antibody (Sigma–Aldrich) and human ApoE ELISA kit (Abcam, Cambridge, MA). Briefly, 10 μL of brain homogenate or 5 μL of CSF (diluted in 50 μL of buffer) was added per well to the anti-ApoE antibody-coated ELISA plate and incubated at 23°C for 2 h. The plate was washed seven times with 200 μL 1× wash buffer (from Abcam ELISA kit). Monoclonal anti-HA antibody, 50 μL per well, was added and incubated at 23°C for 1 h to distinguish the vector expressed human ApoE2-HA protein. The plate was washed seven times with 1× wash buffer. HRP-conjugated goat anti-mouse IgG (Santa Cruz Biotechnology), 50 μL per well, was added and incubated at 23°C for 1 h. The plate was washed seven times with 1× wash buffer. The plate was then incubated with 50 μL per well of HRP substrate (Abcam) at 23°C in the dark for 20 min. The reaction was stopped by adding 50 μL stop solution, and absorbance was read at 450 nm. Total protein in the brain homogenate was measured using micro-bicinchoninic acid kit (Thermo Fisher Scientific, Waltham, MA). The ApoE2-HA level was expressed as ng/mg total protein.

Human ApoE2-HA Western blot analysis

Assessment of transgene expression of human ApoE2-HA protein in the CSF was performed at 0, 4, and 8 weeks post administration of AAVrh.10hAPOE2-HA. CSF was analyzed in a 4–12% polyacrylamide-SDS gel with a standard volume of 10 μL per lane, and transferred onto a polyvinylidene fluoride membrane. The membrane was treated with monoclonal anti-HA antibody, 0.5 μg/mL in 5% dry milk in PBS (Sigma–Aldrich) for 12 h at 4°C and then washed four times with PBS-Tween. The membrane was then incubated with 1:10,000 diluted HRP-conjugated goat anti-mouse IgG (Santa Cruz Biotechnology) for 1 h at 23°C, washed five times with PBS-Tween, and developed with Enhanced Chemiluminescence Plus reagent (Thermo Fisher Scientific). Protein molecular weights on denaturing gels were determined by comparison with the kaleidoscope molecular weight marker standard (Bio-Rad, Hercules, CA).

IHC

The formalin-fixed brains (left hemispheres) were divided into 3 mm coronal slices, embedded in paraffin blocks, and sectioned at 5 μm with a microtome. Every other coronal section (12/21) was examined by IHC, using an anti-HA antibody and counterstain. A standardized subset of sections from animals NHP-10–NHP-14 was additionally stained with H&E for histopathology. IHC staining for HA was performed at the Laboratory of Comparative Pathology on a Leica Bond RX automated stainer (Leica Biosystems, Buffalo Grove, IL). Following heat-induced epitope retrieval (HIER) at pH 6.0, the primary antibody (ab130275; Abcam) was applied at a concentration of 1:2,500 and followed by application of a polymer detection system (DS9800, Novocastra Bond Polymer Refine Detection; Leica Biosystems) in which the chromogen was 3,3 diaminobenzidine tetrachloride (DAB) and the counterstain was hematoxylin. Comparison of the APOE2-HA biodistribution was made on the brain coronal sections by digitizing the IHC slides using high-resolution slide scanning (40×) using a Leica SCN400 scanner (HistoWiz, Brooklyn, NY).

Additional post-IHC processing was done for the intrahippocampal route results (NHP-1 and –2) only. Following IHC processing of the brain coronal sections, the slides were digitized using a Leica SCN400 scanner, and the scan image files were converted to .tif files using ImageScope v12.1 (Aperio Technologies, Vista, CA). Matching IgG control slides were used to remove the background from the .tif images, by setting the negative controls as masks in Adobe PhotoShop. The background subtracted images were then analyzed with ImageJ v1.51n with a heatmap plugin. Gray colors were used in place of purple for the heatmap generation to provide better contrast.

Statistical analysis

All statistical analyses were performed with GraphPad Prism v6.02 (GraphPad Software, San Diego, CA). Analyses comparing the different administration route cohorts to non-treated controls for ApoE2 levels in the CNS were generated using one-way analysis of variance (ANOVA) with Dunnett's multiple comparisons test. Analysis of NHP behavior was carried out by two-way repeated measures ANOVA with Dunnett's multiple comparisons test. Evaluations of CSF ApoE2-HA, blood counts, and serum chemistries were performed by a two-tailed unpaired *t*-test at various time points to identify significant differences due to time. Due to the small sample size ($n = 3$/group) and daily variations in cell numbers and serum chemistries, statistical comparisons were considered to be significant if $p < 0.01$.[31,37,38]

RESULTS

Assessment of AAVrh.10hAPOE2-HA distribution in the CNS

The efficacy of *APOE2* delivery to the CNS in an APOE4 mouse model has been previously demonstrated.[26] The aims of the present study were twofold: (1) to determine the route of delivery that would provide maximum distribution of AAV-mediated *APOE2* vector DNA, transgene mRNA, and ApoE2 protein in the CNS of NHPs; and (2) to assess the safety of these delivery routes. To distinguish the vector-derived APOE2 from endogenous primate APOE2 in immunohistochemical and quantitative assays, a HA peptide tag was added to the 3′ terminus of hAPOE2 vector construct (AAVrh.10hAPOE2-HA). Three routes of vector administration of AAVrh.10hAPOE2-HA in the CNS of NHPs were evaluated (Tables 1 and 2): direct intraparenchymal administration to three sites in the hippocampal region (IH, intrahippocampal); intracisternal (IC, cisternae magna); and intracerebral ventricular (ICV, frontal horn of the third ventricle; Supplementary Fig. S1A). The animals ($n = 3$/route, except for intrahippocampal route, $n = 2$) were euthanized at 8 weeks following vector administration and evaluated by quantitative real-time PCR assessments of *APOE2* DNA and mRNA, and ELISA for protein biodistribution to determine spread and persistence of ApoE2 expression.

Table 1. *Design of the NHP study*[a,b,c,d]

Animal #	*Vector*[e]	*Route of administration*	*Total vector dose (gc)*	*Time of sacrifice (week)*[i]
1 and 2	AAVrh.10hAPOE2-HA	Intrahippocampal[f]	5.0×10^{12}	8
3–5	AAVrh.10hAPOE2-HA	Intracisternal[g]	5.0×10^{13}	8
6–8	AAVrh.10hAPOE2-HA	Intraventricular[h]	5.0×10^{13}	8
9	None (sham)	None	None	8

[a]All NHPs were male African Green monkeys approximately 4–8 years old, weighing around 5–8 kg. MRI scans were performed before surgery to determine administration coordinates for intrahippocampal and intraventricular routes (NHPs 1, 2, 6, 7, and 8).

[b]At pre, 0, 1, 2, 4, and 8 weeks post-vector administration, behavioral assessments were performed with videotaping at rest and in response to a series of standardized challenges with assessment of quantitative traits.[31]

[c]At pre, 0, 1, 2, 4, and 8 weeks post-vector administration following the behavioral assessment (footnote b), the NHPs were sedated with assessment of standard safety parameters, including temperature, pulse, respiratory rate, and weight. Times for assessment up to 2 weeks were ±1 day, and times >2 weeks were ±3 days.

[d]At pre, 0, 1, 2, 4, and 8 weeks post-vector administration, when the NHPs were sedated for assessment of safety parameters (footnote c), blood was sampled for complete blood count, serum chemistry, and neutralizing antibody titers. CSF obtained from the cisterna magna (~500 μL) was sampled, pre-administration, at 4 weeks, and on the day of sacrifice (8 weeks). Times for assessment up to 2 weeks were ±1 day, and times >2 weeks were ±3 days.

[e]NHPs received AAVrh.10hAPOE2-HA formulated in PBS. In order to differentiate vector-mediated expression of APOE2 over the endogenous APOE2 in the NHP brain, the human APOE2 was HA-tagged on the 3′ terminus.

[f]Intrahippocampal route. The vector was administered directly to the NHP hippocampal region, bilaterally, with the volume of the vector delivered at three sites per hemisphere (hippocampus CA1, dentate gyrus, and entorhinal cortex), 15 μL per injection site (infusion rate 1 μL/min), 8.33×10^{11} gc/site.

[g]Intracisternal vector route. The vector was administered directly into the cisterna magna as one single bolus, diluted in 1.5 mL and infused at 0.5 mL/min, followed by a 0.5 mL saline lock flush to ensure delivery of residual vector in the needle/hub.

[h]Intraventricular vector route. The vector was administered as one single dose (1 mL) via a surgically placed catheter in the frontal horn of the lateral ventricle (3rd), unilaterally, and infused at rate of 200 μL/min.

[i]All animals were sacrificed 8 weeks post-vector administration. CSF was sampled for ApoE2-HA analysis. At necropsy, animals were perfused with ice-cold PBS. The brain was divided into two hemispheres, with the left half used for histology and the right half subdivided into cubes (1 cm^3) for biodistribution of vector genome copies, transgene mRNA, and ApoE2-HA protein. Other major organs (lung, liver, heart, spleen, kidney, ileum, and sections of spinal cord—cervical, thoracic, and lumbar) were collected and assessed for gross abnormalities; samples were flash-frozen in liquid nitrogen and stored at –80°C for future use.

NHP, nonhuman primate; gc, genome copies; MRI, magnetic resonance imaging; CSF, cerebrospinal fluid; PBS, phosphate-buffered saline.

Direct intraparenchymal administration

Direct intraparenchymal vector administration was carried out via surgical placement of a catheter into the hippocampus and the entorhinal cortex of

Table 2. *Additional NHP cohorts for toxicity assessment of administration of AAVrh.10hAPOE2-HA*[a,b,c,d]

Animal #	*Vector*[e]	*Route of administration*	*Total vector dose (gc)*	*Time of sacrifice (weeks)*[g]
10–12	AAVrh.10hAPOE2-HA	Intraventricular + intracisternal[f]	1.0×10^{14}	8
13 and 14	None (PBS)[h]	None	None	1–8

[a]All NHPs were male African Green monkeys approximately 4–8 years old, weighing around 5–8 kg. MRI scans were performed before surgery to determine administration coordinates for intraventricular routes and at 8 weeks post administration for safety.

[b]At pre, 0, 1, 2, 4, and 8 weeks post-vector administration, behavioral assessments were performed with videotaping at rest and in responses to a series of standardized challenges with extraction of quantitative traits.[31]

[c]At pre, 0, 1, 2, 4, and 8 weeks post-vector administration following the behavioral assessment (footnote b), the NHPs were sedated with assessment of standard safety parameters, including temperature, pulse, respiratory rate, and weight. Times for assessment up to 2 weeks were ±1 day, and times >2 weeks were ±3 days.

[d]At pre, 0, 1, 2, 4, and 8 weeks post-vector administration, when the NHPs were sedated for assessment of safety parameters listed (footnote c), blood was drawn for complete blood count, serum chemistry, and neutralizing antibody titers. CSF obtained from the cisterna magna ($\sim$500 mL) was sampled for analysis pre-administration, at 4 weeks, and on the day of sacrifice (8 weeks). Times for assessment up to 2 weeks were ±1 day, and times >2 weeks were ±3 days.

[e]NHPs received AAVrh.10hAPOE2-HA formulated in PBS. In order to differentiate vector-mediated expression of APOE2 over the endogenous ApoE2 in the NHP brain, the human APOE2 was HA-tagged on the 3′ terminus.

[f]Dual administration combination route. In these NHPs ($n=3$), the vector was administered via both intracisternal and intraventricular routes (5×10^{13} gc/route), with the surgical placement of catheter and intraventricular delivery performed first, followed by the intracisternal delivery within 15 min following the completion of the intraventricular delivery. In NHP-10 and NHP-12, the intraventricular administration catheter was placed into the left hemisphere; while in NHP-11, the intraventricular administration catheter was placed into the right hemisphere. This was done for a safety risk assessment of 10^{14} gc dosage.

[g]All animals were sacrificed at 8 weeks post-vector administration. CSF was drawn as in footnote d. At necropsy, animals were perfused with ice-cold PBS. The brain was divided into two hemispheres, with the left half used for histology and the right half subdivided into cubes (1 cm^3) for additional studies as needed. Other major organs (lung, liver, heart, spleen, kidney, ileum, and sections of spinal cord—cervical, thoracic, and lumbar) were collected and assessed for gross abnormalities and samples flash-frozen in liquid nitrogen and stored at –80°C for future use.

[h]These two NHPs are historical controls from previous studies where the animals were administered PBS via catheters in the frontal lobe white matter regions, locations that are similar to the path of the intraventricular catheters.[3] They were included for safety assessments at specific time points for hematologic, serum chemistry, serum antibody titers, behavior, and MRI parameters. Additionally, data from 26 NHPs used in previous studies were compiled to generate reference ranges for these safety parameters in male African Green monkeys.[31,35]

the NHP CNS. Administration of 5×10^{12} gc of AAVrh.10hAPOE2-HA directly into the hippocampus/entorhinal cortex achieved easily detectable, diffuse ApoE2 expression (yellow to orange colors on the pseudo-colored heat maps) in targeted regions using this route of delivery compared to the non-treated controls (Supplementary Fig. S2). To prevent inflammatory responses to very high focal vector concentration in the hippocampal area, the vector was administered at 1-log lower total titers and 1/67th volume per deposit. These animals were also monitored for various safety parameters (hematology and serum chemistry) and behavior over an 8-week period post administration. No adverse events or abnormal results were noted.

Intracisternal and intraventricular routes

Although direct administration to the hippocampal/entorhinal cortex provided ApoE2-HA expression in the area of the brain demonstrating the initial pathology of AD,[39–42] Alzheimer's progresses to other areas of the brain.[20,43,44] In addition, administration to the hippocampus/entorhinal cortex requires a complex surgical procedure, and trauma/hemorrhage in this area could have profound consequences.[45–48] With this background, the ability of the less invasive intraventricular or intracisternal administration was explored to mediate expression not only to the hippocampus/entorhinal cortex but also throughout the CNS. To evaluate these routes, at 8 weeks, the brains were evaluated for extent of vector distribution (vector DNA), vector expression (*APOE2-HA* mRNA), and protein (anti-HA ELISA). As expected for a secreted protein such as ApoE2, diffuse expression was observed throughout the CNS. To visualize the extent of vector distribution and expression, a 3D representation of 1 cm^3 cubes of the CNS was used to display the distribution pattern for vector DNA, transgene mRNA, and ApoE2 protein. An example is shown in Fig. 2. For both the intracisternal and the intraventricular routes, for each parameter, greater than baseline levels of vector APOE2-HA copies (Fig. 2A and B), mRNA transgenes (Fig. 2C and D), and ApoE2-HA protein (Fig. 2E and F) were observed in most cubes throughout the CNS, as well as in the hippocampal regions.

Comparison of the distribution of vector DNA, *APOE2-HA* mRNA, and ApoE2-HA protein levels in individual brain cubes of the three NHPs treated with the vector via the intracisternal route and the three NHPs treated with the intraventricular routes demonstrated broad distribution by both routes in all animals compared to the control (Fig. 3A–C). While there was variation in the vector distribution and expression, on average, both the intracisternal and the intraventricular routes provided excellent distribution of the vector and vector expression throughout the CNS compared to the untreated control (Fig. 3D–F). The intracisternal route provided higher vector distribution compared to the intraventricular route ($p<0.001$; Fig. 3D), but

the mRNA and protein expression were similar by the two routes (mRNA $p > 0.5$, protein $p > 0.7$; Fig. 3E and F).

Grouping the individual brain cube vector genome, mRNA, and protein levels in bins of similar levels, quantification of the percentage of positive cubes demonstrated that for the intracisternal route, 92.0% of cubes had vector levels >1,000 copies/μg DNA compared to 3.9% of the control cubes, 81.3% of cubes had vector derived mRNA levels >1,000 copies/μg DNA compared to 2.9% of control cubes, and 68.1% of cubes had vector-derived protein levels >22 ng/mg compared to 3.0% of control cubes (Table 3). The same pattern was observed for the intraventricular route (treated, DNA 90.0% cubes, control 3.9% cubes; mRNA treated 86.0% cubes, control 2.9% cubes; and protein 51.5% cubes, control 3.0% cubes; Table 3). Comparison of the intracisternal versus intraventricular routes demonstrated similar results for all cube parameters (DNA, intracisternal-treated 92.0% of cubes, intraventricular-treated 90% of cubes ($p > 0.6$); mRNA, intracisternal-treated 81.3% of cubes, intraventricular-treated 86.0% of cubes ($p > 0.5$); and protein, intracisternal-treated 68.1% of cubes, intraventricular-treated 51.5% of cubes ($p > 0.5$).

IHC assessment of ApoE2-HA expression in the CNS

To complement the quantification of ApoE2-HA expression in the brain cubes and to identify expression at a cellular level, the left hemisphere and spinal cord were sliced in 3 mm coronal sections and processed for histopathological (H&E) and immunohistochemical analysis (using an anti-HA antibody). To assess the extent of ApoE2-HA distribution across the CNS, coronal slices were analyzed by anti-HA IHC.

When the AAVrh.10hAPOE2-HA vector was delivered to the CSF via the cisterna magna or frontal horn of the third ventricle (the posterior and anterior aspect of the brain, respectively), vector delivery clearly demonstrated ApoE2-HA expression far beyond the local regions of delivery (Supplementary Figs. S3–S5). The brains from the intracisternal and intraventricular administration groups showed areas of ApoE2-HA expression in a wide range of brain regions from the anterior to the posterior. There was heavy staining of the ependymal cells of the choroid plexus in the ventricles, as expected due to the routes of delivery into the CSF (Supplementary Figs. S3–S5) but also in areas around the frontal and mid-brain, including the hippocampal region, as well as areas around the posterior of the brain and spinal cord. Regions associated with early AD in humans (hippocampus, entorhinal/parahippocampal cortex) were appraised for ApoE2-HA for each monkey in the study. The cytoplasm of neuronal cell bodies and neuropil displayed intense staining ApoE2-HA in the targeted areas, including the parahippocampal cortex, entorhinal cortex, parasubiculum, dentate gyrus, and CA1 of hippocampus (Supplementary Figs. S3 and S4F–I). In contrast, no ApoE2-HA expression was observed in the brains from the non-treated control NHP (Supplementary Fig. S5A–O). Comparisons of the staining observed in the intraventricular and intracisternal routes revealed little differences in the overall APOE2-HA expression patterns across the CNS, with the exception that concentrated staining was observed for ApoE2-HA in the lateral ventricle (Supplementary Figs. 3SA and S4A) and caudate putamen (Supplemental Figs. S3B and S4B) with the intraventricular route in the area just around the

Figure 2. Example of distribution of *APOE2* vector genome copies, transgene mRNA, and protein levels in the brains of nonhuman primates (NHPs) administered with AAVrh.10hAPOE2-HA via intracisternal or intraventricular routes. Shown are data from NHP-4 for the intracisternal route and NHP-8 for the intraventricular route. The distribution of *APOE2* vector genome copies, transgene mRNA copy numbers, and protein is represented by three-dimensional schematic drawings of 1 cm^3 cubes of the right hemispheres. African Green monkeys administered AAVrh.10hAPOE2-HA (5×10^{13} genome copies [gc]) as described in Table 1 were euthanized 8 weeks post surgery. The right hemispheres were subdivided into 1 cm^3 cubes, homogenized, and analyzed for vector genome copies and transgene mRNA by quantitative polymerase chain reaction and analyzed for protein ApoE2-HA levels by enzyme-linked immunosorbent assay (ELISA). Coronal slices (1 cm width) are displayed from the anterior to the posterior end of the NHP brains, with the subdivided cubes recreated for each coronal slice. **(A**, **C**, and **E)** Intracisternal (IC) route. **(B**, **D**, and **F)** Intraventricular (ICV) route. In panels **(A)** and **(B)**, the cube colors are based on the mean vector genome TaqMan levels (# cDNA gc/mg DNA): *light yellow*, background ($<10^3$ copies); *blue*, 10^3–10^4 copies; *green*, 10^4 to 5×10^4 copies; *red*, 5×10^4 to 10^5 copies; *purple*, $>10^5$ copies; *gray*, insufficient sample for analysis. In panels **(C)** and **(D)**, the cube colors are based on the mean transgene mRNA TaqMan readings/cube (# mRNA copies [gc]/mg DNA): *light yellow*, background levels ($<10^3$ copies); *blue*, 10^3 to 10^4 copies; *green*, 10^4 to 5×10^4 copies; *red*, 5×10^4 to 10^5 copies; *purple*, $>10^5$ copies; *gray*, insufficient sample for analysis. In panels **(E)** and **(F)**, the cube colors are based on the mean ApoE2-HA ELISA levels/cube (ApoE2-HA [ng]/mg total protein): *light yellow*, background levels; *blue*, >0.1–22 ng/mg; *green*, 22–50 ng/mg; *red*, 50–100 ng/mg; *purple*, >100 ng/mg; *gray*, insufficient sample for analysis. The baseline values for ApoE2-HA protein were based on the mean $\pm 2SD$ for the untreated control cubes (21.42 ng/mg protein). *Black arrows* denote the location of the catheter insertion site for each route. Relative locations of the hippocampal region are shown by *yellow arrows*. The percentage cubes positive for each category (see Table 3) was calculated based on total cubes analyzed for each monkey (70 and 80 cubes per brain). Schematic of primate brain, right hemisphere is shown as reference to coronal sections used for the analysis of cubes.

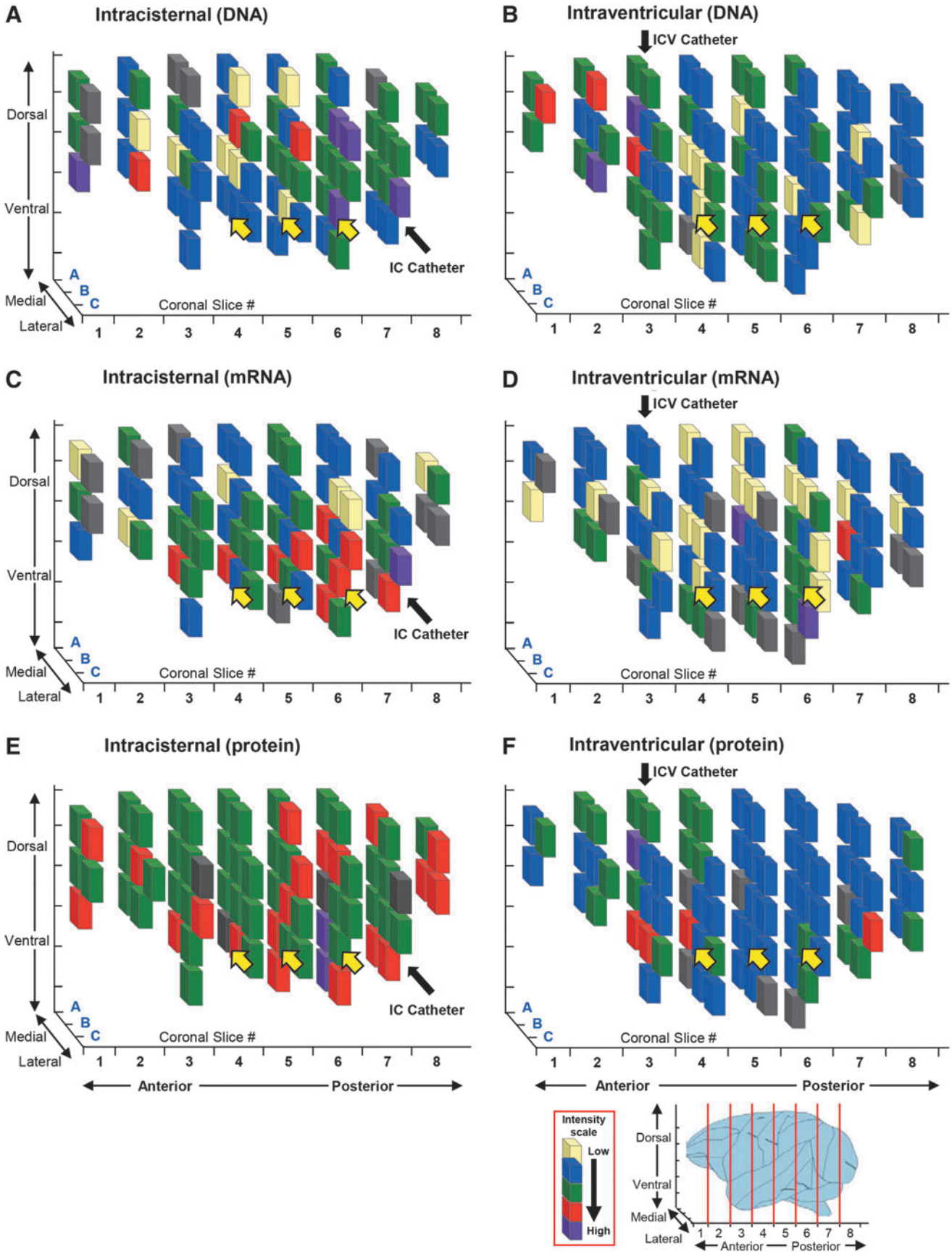
A
Intracisternal (DNA)
Dorsal
Ventral
Medial
Lateral
IC Catheter
A
B
C
Coronal Slice #
1 2 3 4 5 6 7 8
B
Intraventricular (DNA)
ICV Catheter
C
Intracisternal (mRNA)
D
Intraventricular (mRNA)
E
Intracisternal (protein)
F
Intraventricular (protein)
Anterior
Posterior
Intensity scale
Low
High

catheter placement for this route of delivery. Beyond the expected staining in the targeted areas of the chronic plexus of the ventricles (Supplementary Figs. S3C and S4C), staining was observed in numerous substructures across the CNS, including the anterior olfactory nucleus, thalamic reticular nucleus, lateral hypothalamus, pineal body in the epithalamus, stria terminalis, pontine gray fibers in the brain stem, Purkinje cells and deep cerebellar nuclei in the cerebellum and gray nuclei of the spinal cord (Supplementary Figs. S3 and S4D, E, and J–O), as well as multiple substructures in the brain stem (not shown). Due to their involvement in early detection of AD,[49,50] the olfactory bulb and visual cortex regions were additionally compared for effect of route of treatments (Supplementary Fig. S6A–L). Multiple layers of the olfactory bulb/nucleus and occipital visual cortex displayed positive ApoE2-HA staining.

ApoE2-HA expression in the CSF over time

As an additional measure of efficacy, levels of ApoE2-HA in the CSF were assessed by Western blot analysis and ELISA at day 0 (pre-therapy), day 28, and day 56 (prior to necropsy; Fig. 4). Both routes of delivery, intracisternal (Fig. 4A) and intraventricular (Fig. 4B) displayed an abundance of circulating ApoE2-HA in the CSF at each post-administration time point, demonstrating long-term expression through the life of the study (8 weeks). Quantification of ApoE2-HA in the CSF by ELISA demonstrated consistent levels >1 μg/mL CSF protein above endogenous background levels at both time points sampled post vector administration in NHPs by both routes. There was no significant difference between the two routes ($p > 0.9$).

Safety studies

As a "worst-case" scenario and to minimize the use of NHPs, three NHPs were administered the vector via the dual route (intraventricular and intracisternal) using a total of double the prior vector dose (10^{14} gc) and volume (2 mL) delivered into the CSF (Table 2). Multiple regions from samples across the brain were selected and stained with H&E for microscopic examination of the areas proximal and distal to the catheter needle insertions for each route (see sampling schematic, Supplementary Fig. S7). Overall gross and microscopic pathology showed no effects of the dose/volume (5×10^{13} gc and 1 mL of vector per CSF site) of vector beyond focal superficial parenchymal loss due to surgical intervention, similar to that observed in previous studies with PBS-treated controls.[31] Histopathological examination of the brain left frontal lobes from the dual-route NHPs (NHP-10–NHP-12) revealed focal lesions in the gray matter with minor histiocytic

Figure 3. Quantitative comparison of intracisternal versus intraventricular routes of AAVrh.10APOE2-HA administrated to the CNS of NHPs. The distribution of *APOE2-HA* vector genome copies, transgene mRNA copy numbers, and protein levels in the brains of NHPs administered with AAVrh.10hAPOE2-HA or non-treated animals are shown for all intracisternal and intraventricular NHPs in the study. African Green monkeys ($n=6$ and $n=3$/route) were administered AAVrh.10hAPOE2-HA (5×10^{13} gc) or were untreated ($n=1$, sham control), as described in Table 1 and Fig. 2. **(A–C)** All data displayed for each NHP separately. **(D–F)** All data for all NHPs in each route grouped together. **(A)** Vector genome copies, all individual NHP data. The extent of distribution above background assay levels is shown (10 copies). All cube results were assembled into one set per NHP to show overall vector genome copy numbers. Intracisternal NHP cubes, *circles*; intraventricular NHP cubes, *triangles*; untreated control, *inverted triangles*. Means are shown by *solid black lines* in each NHP set. The *dashed lines* represent the levels used for analysis in Fig. 2 and Table 3, and the ranges are based on the mean gDNA TaqMan levels (#gc/mg DNA): $<10^3$ copies; 10^3 to 10^4 copies; 10^4 to 5×10^4 copies; 5×10^4 to 10^5 copies; and $>10^5$ copies. **(B)** Human *APOE2* transgene mRNA copies, all individual NHP data. The extent of APOE2 mRNA expression distribution above background assay levels is shown (10 copies). All cube results were assembled into one set per NHP to show overall mRNA copy numbers. Intracisternal NHP cubes, *circles*; intraventricular NHP cubes, *triangles*; untreated control, *inverted triangles*. Means are shown by *solid black lines* in each NHP set. The *dashed lines* represent levels used for analysis in Fig. 2 and Table 3, and the ranges are based on the mean mRNA TaqMan levels (# copies [gc]/mg cDNA) $<10^3$ copies; 10^3 to 10^4 copies; 10^4 to 5×10^4 copies; 5×10^4 to 10^5 copies; and $>10^5$ copies. **(C)** Human ApoE2 protein (HA-tag), all individual NHP data. The extent of ApoE2 expression in the brain cubes above background assay levels is shown (1 ng/mg). All cube results were assembled into one set per NHP to show overall ApoE2-HA levels. Intracisternal NHP cubes, *circles*; intraventricular NHP cubes, *triangles*; untreated control, *inverted triangles*. Means are shown by *solid black lines* in each NHP set. The baseline values for ApoE2-HA protein were based on the mean $\pm 2SD$ for the untreated control cubes (21.42 ng/mg protein). The *dashed lines* represent levels used for analysis in Fig. 2 and Table 3, and the ranges are based on the mean protein ELISA levels/cube: <22 ng/mg, 22–50 ng/mg, 50–100 ng/mg, and >100 ng/mg protein. **(D)** Vector genome copies, all NHP data combined. The combined data from all NHPs per route of vector administration for vector genomes are shown. All cube results were assembled into one set per treatment for comparisons, with intracisternal NHP cubes, *red circles*; intraventricular NHP cubes, *blue triangles*; untreated control, *yellow inverted triangles*. Means are shown by *solid black lines*, with the same *dashed line* ranges as in **(A)**. **(E)** Human *APOE2* mRNA copies, all NHP data combined. The combined data from all NHPs per route of vector administration for mRNA copy number are shown. The graph displays the combined data from all NHPs per route of vector administration for vector genomes. All cube results were assembled into one set per treatment for comparisons, with intracisternal NHP cubes, *red circles*; intraventricular NHP cubes, *blue triangles*; untreated control, *yellow inverted triangles*. Means are shown by *solid black lines* in each treatment, with the same *dashed line* ranges as in **(B)**. **(F)** Human ApoE2 protein (HA-tag), all NHP data combined. The combined data from all NHPs per route of vector administration for ApoE2 protein expression are shown. The graph displays the combined data from all NHPs per route of vector administration for vector genomes. All cube results were assembled into one set per treatment for comparisons, with intracisternal NHP cubes, *red circles*; intraventricular NHP cubes, *blue triangles*; untreated control, *yellow inverted triangles*. Means are shown by *solid black lines* in each treatment, with the same *dashed line* ranges as in **(C)**. Statistical comparison of the treatment routes and controls were calculated by an unpaired two-sided Student's *t*-test, with alpha <0.05.

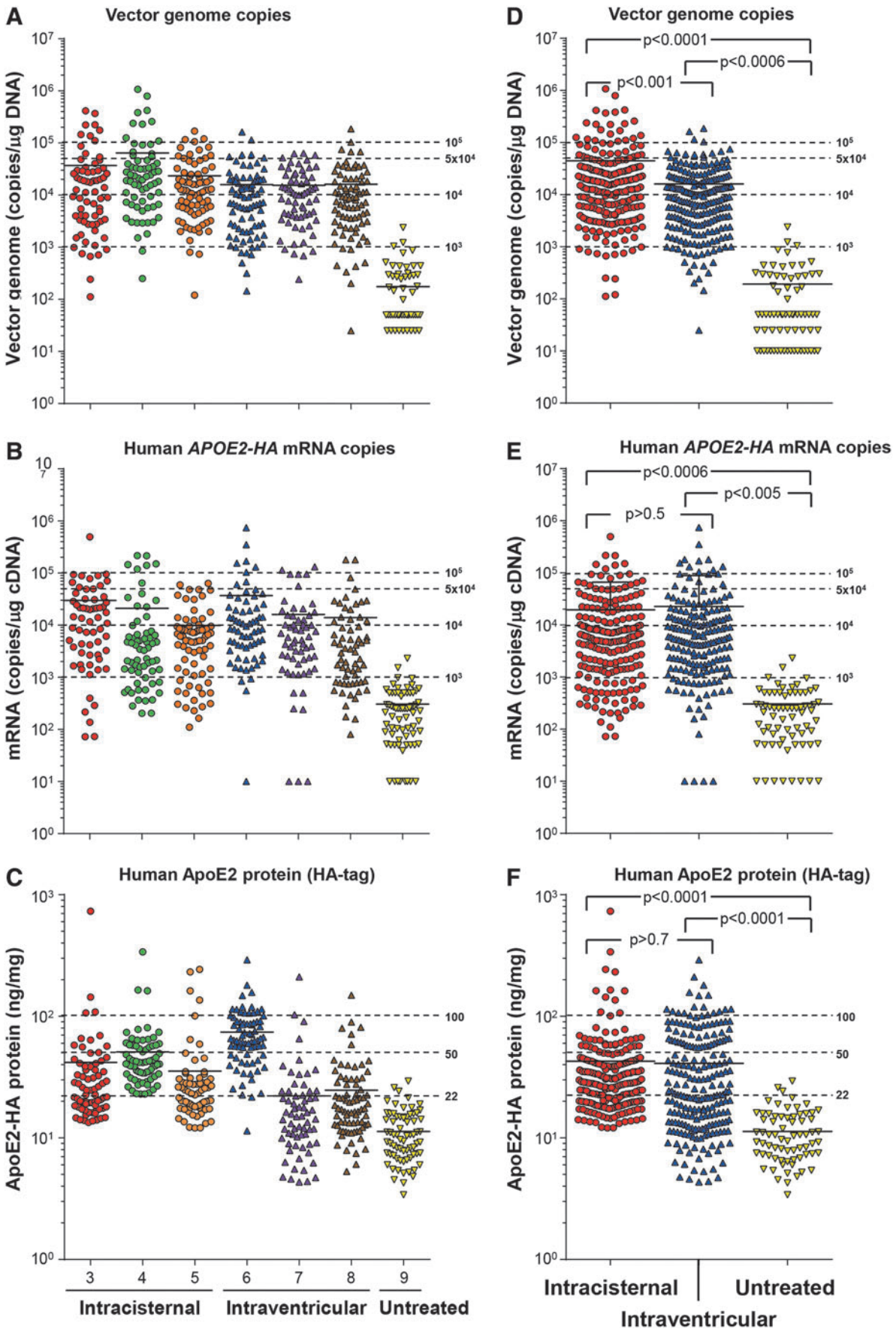
A
Vector genome copies
Vector genome (copies/µg DNA)
B
Human APOE2-HA mRNA copies
mRNA (copies/µg cDNA)
C
Human ApoE2 protein (HA-tag)
ApoE2-HA protein (ng/mg)
3 4 5 6 7 8 9
Intracisternal
Intraventricular
Untreated
D
Vector genome copies
p<0.0001
p<0.0006
p<0.001
E
Human APOE2-HA mRNA copies
p<0.0006
p<0.005
p>0.5
F
Human ApoE2 protein (HA-tag)
p<0.0001
p<0.0001
p>0.7
Intracisternal
Untreated
Intraventricular

Table 3. *Comparison of intracisternal versus intraventricular routes of delivery of AAVrh.10hAPOE2-HA as assessed by copies of vector genome, copies of transgene mRNA, and ApoE2-HA protein levels*[a]

	% Cubes[b]					
Parameter	*Intracisternal*		*Intraventricular*		*Non-treated*	
Vector genome copies/mg DNA[c]						
$<10^3$	8.0 ± 4.5		10.0 ± 1.0		96.1	
10^3–10^4	35.1 ± 3.3		45.4 ± 1.8		3.9	
10^4–5×10^4	40.6 ± 2.7		38.2 ± 2.8		0.0	
5×10^4–10^5	8.1 ± 1.9	92.0%	5.2 ± 0.8	90.0%	0.0	3.9%
10^5–10^6	7.7 ± 2.4		1.3 ± 0.7		0.0	
$>10^6$	0.5 ± 0.5		0.0 ± 0.0		0.0	
Transgene mRNA copies/mg cDNA[d]						
$<10^3$	18.7 ± 6.9		14.0 ± 6.5		97.1	
10^3–10^4	49.1 ± 5.1		49.1 ± 2.3		2.9	
10^4–5×10^4	22.7 ± 8.5		28.1 ± 3.9		0.0	
5×10^4–10^5	6.5 ± 4.4	81.3%	3.9 ± 1.7	86.0%	0.0	2.9%
10^5–10^6	3.1 ± 2.3		4.8 ± 1.4		0.0	
$>10^6$	0.0 ± 0.0		0.0 ± 0.0		0.0	
ApoE2-HA protein (ng/mg total protein)[e]						
<22	31.9 ± 16.0		48.5 ± 23.1		97.0	
22–50	50.4 ± 9.2		24.6 ± 1.3		3.0	
50–100	13.9 ± 7.8	68.1%	18.9 ± 16.3	51.5%	0.0	3.0%
100–500	3.4 ± 0.4		8.0 ± 6.5		0.0	
>500	0.5 ± 0.5		0.0 ± 0.0		0.0	

[a]The results in Fig. 3 were analyzed for the number of cubes per expression level group. The data are shown as the percentage of total number of brain cubes analyzed. The vector genome copies, transgene mRNA, and ApoE2-HA protein expression detected in each brain cube were grouped into level bins to display the extent of the levels of vector genome copies, transgene mRNA, and ApoE2 expression in the NHP brains following gene transfer. These artificial bins were established to group similar expression amounts.

[b]Cubes for each parameter were counted, expressed as percentage of total brain cubes per NHP, and then averaged for each treatment. Shown are the mean of $n=3$ NHPs per group ± standard error of the mean, except for the non-treated NHP, where $n=1$. All cubes with insufficient sample for analysis have been removed from the counts.

[c]Vector genome copy number levels are based on the mean DNA copy number/cube (copies/mg DNA).

[d]Transgene mRNA copy number levels are based on the mean mRNA copy number/cube (copies/mg cDNA).

[e]Protein assay results are based on the mean ApoE2-HA protein levels/cube (ApoE2-HA ng/mg total protein). The baseline cut off for ApoE2-HA protein was based on the mean ± 2*SD* for the untreated control (21.42 ng/mg protein).

infiltrate and hemosiderosis in the gray matter (Supplementary Fig. S7A–F) and multifocal gliosis with histiocytic infiltrate, hemosiderosis, spongiosis, and vascular hyperplasia in the underlying white matter (Supplementary Fig. S7G–L). These findings were compatible with a needle tract used to deliver the AAV vector in the intraventricular route and comparable to that observed in PBS-treated animals (NHP-13–NHP-14; Supplementary Fig. S8A–D). Similarly, microscopic examinations of the cerebellum lobes, dorsal to the site of administration for the intracisternal route, displayed no evidence of pathology or inflammation of the cerebellum in the three dual-route administered NHPs (Supplementary Fig. S7M–R). Further examination of CNS regions distal to the intraventricular catheter insertions used for vector administration demonstrated no vector-associated pathology in the brain. Regions assessed included the frontal lobe lateral ventricle (Supplementary Figs. S8E and S9A, E, and I), parietal lobe white matter (Supplementary Figs. S8F and S9B, F, and J), temporal lobe hippocampal region (Supplementary Fig. S9C, G, and K), and occipital lobe visual cortex (Supplementary Fig. S9D, H, and L). No other changes were observed. All other findings were consistent with incidental background lesions that can be expected to occur naturally in animals of this species, age, and sex.

Additional safety parameters

The NHPs underwent routine safety testing, including monitoring for blood parameters (hematologic, serum chemistry, antivector antibody titers), in-life and necropsy parameters, and behavior over 8 weeks post administration.

Analysis of serum demonstrated that administration by both the intraventricular and the intracisternal routes were associated with the development of anti-AAVrh.10 antibodies (Fig. 5A and B). Although the study cohort was small ($n=3$/route), it appears that the intracisternal route in NHPs generated on average slightly lower anti-AAVrh.10 antibodies compared to that of the intraventricular route NHPs. Statistical comparisons between the NHP cohorts showed significance between treated and non-treated groups comparing day 28 and 56 titers for each group by the Student's *t*-test (total antibody titers, intracisternal vs. non-treated, $p<0.01$; intraventricular vs. non-treated, $p<0.04$, intracisternal vs. intraventricular, $p>0.06$; Fig. 5A; neutralizing titers, intracisternal vs. non-treated, $p<0.02$; intraventricular vs. non-treated, $p<0.03$; intracisternal vs. intraventricular, $p>0.06$; Fig. 5B).

Blinded videotape analysis of NHP behavior before surgery and after administration showed no discernible neurological differences in any of the routes tested (Fig. 6). All NHP scores of "healthy" activities (Supplementary Table S1) were within the historic range of normal NHP behavior (Fig. 6A). No adverse effects were observed during the sessions, other than two NHPs displaying stereotypy (scratching and pacing) at both pre- and post-surgery time points (Fig. 6B).

The vector-administered groups (all routes) did not differ from the sham controls ($n=2$) in any parameter of general assessment or comprehensive blood profile (complete blood count and chemistry panel), remaining within the historic ranges obtained

from previous studies (Supplementary Figs. S10 and S11).[31,35] When compared to the historic ranges, there were rare outlier values observed over the course of the study for a small number of hematologic and serum chemistry parameters for both treated animals and controls. Pairwise statistical comparisons between the treated NHPs and non-treated sham controls showed very few parameters with significant p-values ($p < 0.01$), none of which had clinical significance. For the intracisternal vector-treated treated animals, there was a significant difference between treated and control animals for globulin (day 28) and albumin/globulin ratio (day 28). For the intraventricular vector-treated animals, there was significant difference between treated and control animals for WBCs (day 0) and reticulocytes (day 28). For the dual intraventricular/intracisternal vector-treated animals, there was a significant difference between treated and control animals for RBCs (day 0) and hematocrit (days 0, 56). None was vector related. The elevated ALT, AST, and LDH at early time points were most likely surgery and anesthesia related,[51] and all of these resolved (day 56; Supplementary Fig. S11E, F, and G). Similar findings lacked differences for in-life parameters (total body weight, body temperature, heart and respiratory rates; not shown), with a few scattered outliers, with nothing linked to the vector. For the intracisternal vector-treated animals, one of three NHPs had an elevated heart rate (days 7 and 14), and one of three NHPs had an elevated respiratory rate (days 7 and 28). For the dual intraventricular/intracisternal vector-treated animals, one of three NHPs had an elevated heart rate (days 7 and 14). Analogous outcomes were noted following the termination of the experiment. No differences were noted for the necropsy weights between the dual-route (intraventricular plus intracisternal) and PBS-treated controls, other than smaller hearts in the smaller monkeys (not shown).

To assess for any vector- or surgery-related inflammation or acute pathology, the NHPs in the study were evaluated by MRI at two time points: prior to surgery (0 weeks) and prior to necropsy

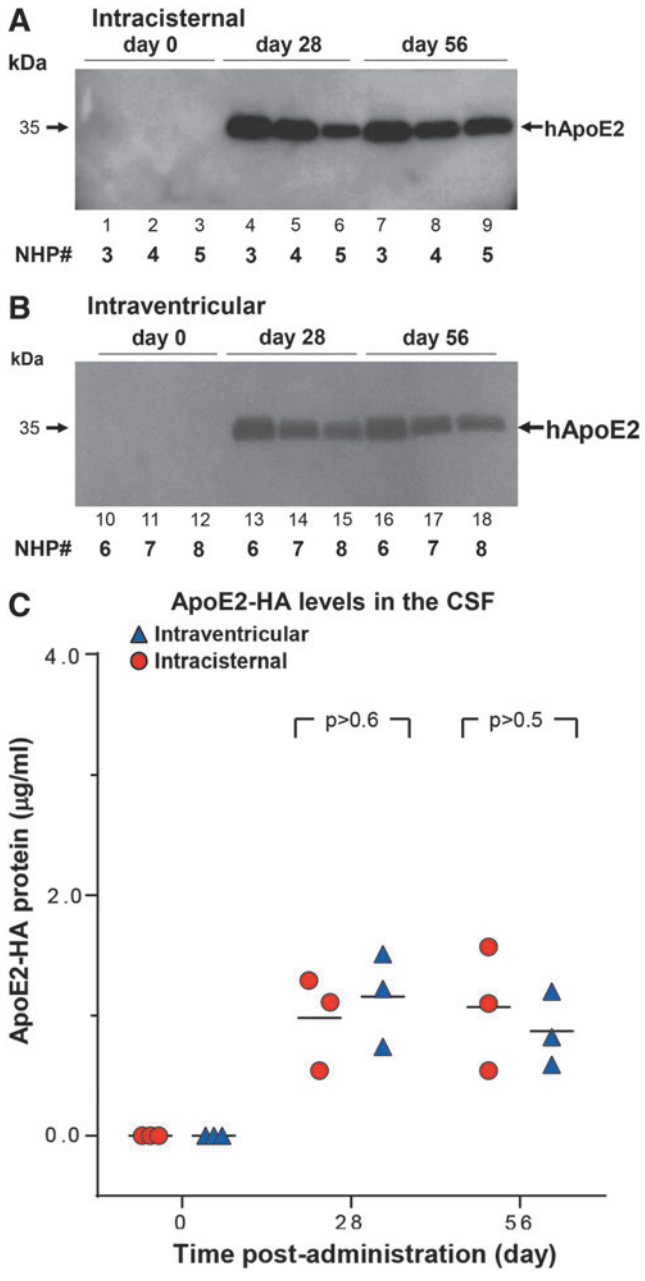

Figure 4. NHP cerebrospinal fluid (CSF) human ApoE2 levels following AAVrh.10hAPOE2-HA administration. CSF was sampled from the NHPs at three time points (pre-administration [day 0] and days 28 and 56 post administration). CSF (10 μL/time point) was analyzed by sodium dodecyl sulfate polyacrylamide gel electrophoresis followed by anti-HA antibody detection by APOE2-HA Western blot and by ApoE2-HA ELISA. **(A)** CSF from NHPs administered via the intracisternal route (NHP-3–NHP-5). Lanes 1–3, day 0; lanes 4–6, day 28; and lanes 7–9, day 56, prior to necropsy. **(B)** CSF from NHPs administered via the intraventricular route (NHP-6–NHP-8). Lanes 10–12, day 0; lanes 13–15, day 28; and lanes 16–18, day 56, prior to necropsy. The "day 28" sample from NHP-3 was collected on day 21. The molecular weight of human APOE2 is shown by the *arrows*. **(C)** ApoE2-HA levels in the CSF detected by ELISA. The same samples from NHP-3–NHP-8 were additionally analyzed by an ApoE2 capture ELISA to quantitate the levels detected by Western blot analysis. The background of the ELISA was subtracted from each sample. The graph displays the three time points (0, 28, and 56 days) assessed for ApoE2-HA in the CSF for each route of vector administration, with intracisternal NHP (NHP-3–NHP-5), *red circles*; intraventricular NHP (NHP-6–NHP-8), *blue triangles*. $M \pm SD$ at day 28: intracisternal, 0.98 ± 0.39; intraventricular, 1.16 ± 0.39 ng ApoE2/mL CSF. $M \pm SD$ at day 56: intracisternal, 1.07 ± 0.52; intraventricular, 0.87 ± 0.31 ng ApoE2/mL CSF. Comparisons between the two administration routes showed no difference concerning the route of treatment: $p > 0.6$, day 28, and $p > 0.5$, day 56, or all time points, $p > 0.9$.

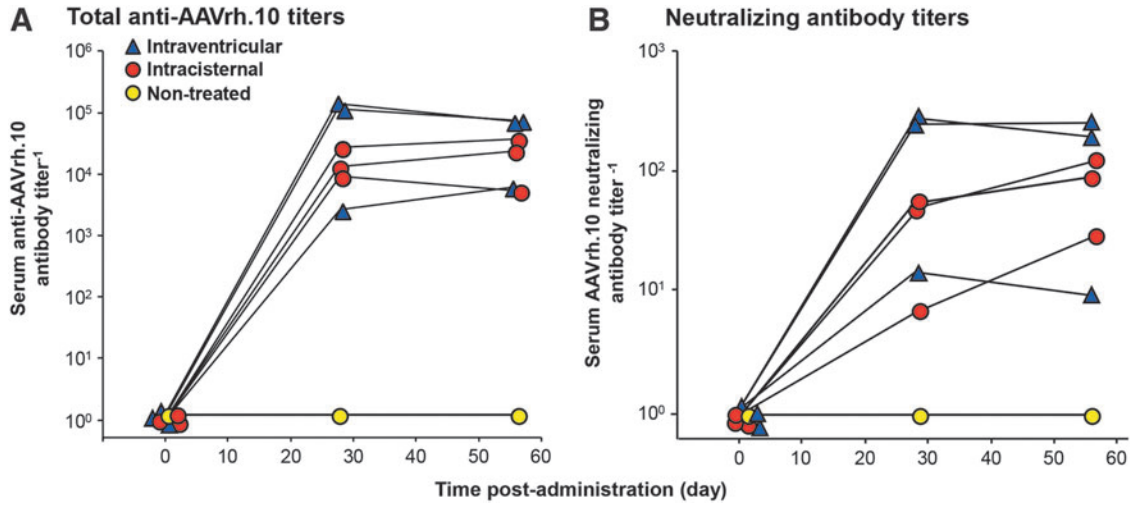

Figure 5. Assessment of total anti-AAVrh.10 and neutralizing anti-AAVrh.10 antibody titers in NHP for humoral response evoked by CNS administration of AAVrh.10hAPOE2-HA. Total anti-AAVrh.10 and neutralizing anti-AAVrh.10 antibody titers in the NHP serum were determined at three time points: before dosing (pre-surgery, day 0), and at 28 and 56 days after vector administration of AAVrh.10hAPOE2-HA ($n=3$/route) or non-treated control ($n=1$). At the indicated time, the NHPs were sedated for blood sampling with assessment of antibody titers in serum. The total antibody titer is expressed as the reciprocal of the serum dilution, while the neutralizing antibody titer is expressed as the reciprocal of serum dilution at which 50% inhibition of AAVrh.10Luc was observed. Shown are the results for each NHP in the study, color-coded by treatment route (*red circles*, intracisternal; *blue triangles*, intraventricular; *yellow circles*, non-treated control). **(A)** Total serum anti-AAVrh.10 antibody titers. **(B)** Serum neutralizing anti-AAVrh.10 antibody titers. Limit of detection is 10^0. Symbols are offset to display each NHP in the study. Comparisons between either of the administration routes and the non-treated NHPs were significant for post-treatment titers but not between the routes of administration (total antibody titers, intracisternal vs. non-treated: $p<0.01$; intraventricular vs. non-treated: $p<0.04$; intracisternal vs. intraventricular, $p>0.06$; neutralizing titers, intracisternal vs. non-treated: $p<0.02$; intraventricular vs. non-treated: $p<0.03$; intracisternal vs. intraventricular, $p>0.06$).

(8 weeks ±3 days). Full-head T1 axial scans were performed without contrast agents on the three dual-route NHPs and one non-treated control (NHP-10–NHP-13; Supplementary Fig. S12A–H). No visual pathology was noted around the administration sites other than thin holes from catheters. No inflammation or pathologic abscesses were discovered on the MRI series. This was confirmed on T2 and T2-FLAIR scans (not shown) during the same imaging session. The routine delivery to the CSF in the NHP brains appears to be well tolerated, even with double the dose and volume in the dual-route applications.

DISCUSSION

Individuals who are *APOE4* homozygotes have a markedly increased risk of developing AD. *APOE2* homozygotes are protected from late-onset AD and, compared to *E4* homozygotes, *APOE2/E4* heterozygotes have a markedly reduced risk of developing AD.[6,12,13] Based on this genetic data, it was hypothesized that expression of the "protective" *APOE2* variant by genetic modification of the CNS of *E4* homozygotes could reverse or prevent the progressive neurologic damage associated with the *APOE4* variant. The efficacy of this approach in AD transgenic mouse models has been demonstrated previously.[23,24,26] To translate this therapy to the clinic, the present study was designed to assess the optimal route of administration and safety of AAVrh.10-mediated delivery of human *APOE2* coding sequence to the CNS.

AAV-mediated gene therapy to the CNS

As the gene therapy field advances with new treatment methods and delivery vehicles, cures for intractable degenerative neurological diseases, such as AD, Parkinson's disease, and Huntington disease, have become a distinct possibility.[22,52–54] Gene therapy using AAV constructs to deliver corrected versions of mutated or missing genes linked to CNS-related diseases has been a hot-bed of activity over the past decade, with many clinical trials underway to evaluate the safety and efficacy of potential AAV-mediated gene therapies, including lysosomal storage disorders (late infantile neuronal ceroid lipofuscinosis [LINCL], metachromatic leukodystrophy [MLD], Pompe disease, Canavan disease, Tay Sachs disease, mucopolysaccharidosis IIIA, and Gaucher's disease), AD, Parkinson's disease, giant axonal neuropathy, and spinal muscular atrophy.[52,53,55–65] Each disease has its own set of hurdles that require tailored extensive preclinical research in animals. The major issues facing suc-

cessful CNS gene therapy involve: (1) optimal vector for expression of the therapeutic, (2) routes of delivery, and (3) safety.

AAV vectors

AAV vector-mediated gene therapy has become a preferred method for delivering therapeutic genes to the CNS.[52,66] AAV vector administration to the CNS has an excellent safety and efficacy profile.[52,53,55–65] Although the gene packaging size is limited (maximum 5.0 kb), typically the relevant gene coding sequences can be easily packaged for CNS delivery.[52,67]

Regarding the AAV serotype for CNS gene therapy, it has been shown that AAV1, AAV8, AAV9, and AAVrh.10 are primarily neurotropic in their transduction capacity,[68] whereas AAV2 is restricted to pyramidal and granular cells,[69] AAV4 is astrocyte and ependymal cell specific[70], and AAV5 transduces only granular cells.[69] Of these AAV serotypes, the most commonly used for clinical trials to date are AAV5, AAV9, and AAVrh.10.[52,56,58,71] In prior studies, AAVrh.10 was found to be superior for widespread CNS expression than several serotypes, including AAV5.[27,32] For the current Alzheimer's APOE2 study in NHPs, the choice of AAVrh.10 as a gene delivery vector was based on the following: (1) comparison of multiple AAV serotypes demonstrated that AAVrh.10 provided wide distribution and high levels of transgene expression in the brain; (2) pre-existing antivector immunity in humans is minimal because AAVrh.10 is derived from rhesus macaques[72]; (3) previous toxicology studies designed in concordance with the Food and Drug Administration established the safety of AAVrh.10 as a gene delivery vehicle in small- and large-animal species as a prerequisite for testing in the human brain; and (4) AAVrh.10-based vector has been

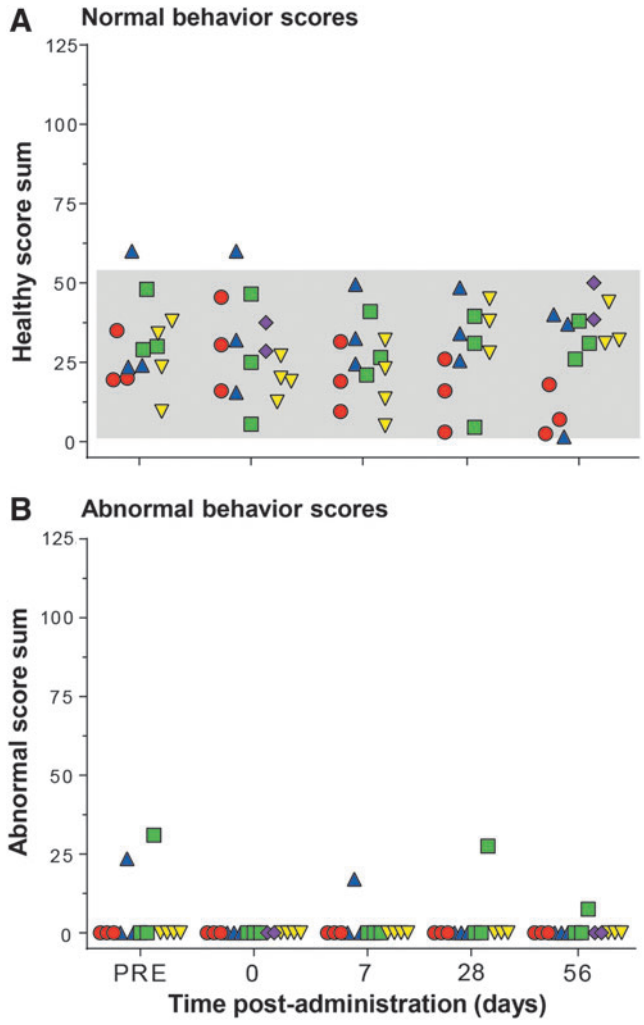

Figure 6. Behavior safety assessment of NHP following CNS administration of AAVrh.10hAPOE2-HA. African Green monkeys were assessed for normal and abnormal behavior parameters at regular intervals before and after surgery (see Supplementary Table S1 for details). At the indicated times, the NHPs were videotaped for all activity, before and after surgery, by monitoring their activity levels and actions to evaluate whether the surgery, route of delivery, and/or vector dose had any effect on health over time. The NHPs were assessed at five time points: >1 week prior to surgery (pre), on the day of administration (day 0), and on days 7, 28, and 56 after administration (prior to necropsy). Times for assessment were ±1 day. Shown are the results of normal and abnormal behavior scores for each NHP in the study, color-coded by treatment (*red circles*, intracisternal route; *blue triangles*, intraventricular route; *green squares*, dual intraventricular + intracisternal route; *purple diamonds*, intrahippocampal route; and *yellow inverted triangles*, sham or non-treated NHPs). The normal range, shown as the *gray-shaded area* for each parameter, was calculated from historic and current African green monkey studies ($n=26$ individual male NHPs and $n=62$ individual behavioral sessions, before surgery),[31,35] as the mean ± 2*SD* of each overall score sum of monkeys in the studies at the presurgical time point ("pre" and day 0, prior to surgery or vector administration). At each time point, each animal was videotaped for 3 min in the absence of outside stimuli and subsequently analyzed by two blinded observers for 20 specific primate behaviors (normal, $n=14$; abnormal, $n=6$), scoring "1" for 5 s of each behavior. The sum of normal typical primate behaviors observed during each session was calculated as a "healthy" score (see Supplementary Table S1 for details) for each session and plotted as the $M \pm SD$ as a function of time. Similarly, the sum of all abnormal observed behaviors was calculated as an "abnormal" score (see Supplementary Table S1 for details) for each session. **(A)** Healthy sum scores. No differences were seen between the non-treated controls versus AAV-treated NHP for any route of delivery (one-way analysis of variance with Dunnett's multiple comparisons test): non-treated versus intracisternal, $p>0.2$; non-treated versus intraventricular, $p>0.4$; non-treated versus dual routes, $p>0.9$; non-treated versus intrahippocampal, $p>0.1$. Comparison of the data collected by the two blinded reviewers showed no significant reviewer based difference for any of the NHPs (range $p>0.3$ to $p>0.99$). **(B)** Abnormal sum scores. None of the NHP showed abnormal behaviors other than three incidents of stereotypy (scratching and continuous pacing) observed in two NHP, which was the same behavior pattern observed in the same NHP at pre- and post-vector administration.

administered to the brain of children with MPS-IIIA in clinical trials with no drug-related clinically relevant adverse events up to 4 years following treatment.[58,73]

Routes of AAV vector delivery

There are multiple routes available for vector-mediated delivery of the therapeutic transgene into the CNS, and each has its pros and cons. The most common route is direct administration to the brain parenchyma (intraparenchymal route), which involves delivering the vector to the sites of need or local gene expression, such as the subthalamic nucleus (Parkinson's)[74] or white matter (LINCL and MLD).[75,76] The advantage of this route is the directed gene delivery to specific targeted brain regions. However, there are disadvantages, including limited vector delivery amounts and volumes, limited spread of the vector in confined space, pathology to regions of important brain functions from the catheters or localized high concentration of the vector, and the requirement for invasive surgery with weeks of postoperative recovery. To overcome the limited vector spread, studies have been carried out to assess delivering the vectors to multiple sites along each delivery trajectory during surgery for maximum coverage in the CNS.[31,34,62,64,77] One modified intraparenchymal delivery method in clinical use is convection-enhanced delivery (CED). This has the advantage of increased vector volume that can be delivered to the target site, which enhances cell transduction in the targeted CNS substructure, such as the putamen and caudate nucleus.[78–80] However, the CED strategy has associated localized trauma possible from the surgical intervention and increased pressure of fluid volume due to vector delivery in a confined space. As shown in the data in the present study, the direct intraparenchymal route could be used for AD to deliver directly to the hippocampus, but this will involve delicate surgery to avoid pathology in such a critical structure to obtain coverage in the hippocampal target region.[45–48]

To overcome the issue of surgery-induced pathology following direct vector delivery to the CNS, less invasive routes have been examined. Since the CSF bathes the entire parenchyma, studies have been designed to deliver the viral vectors to the CSF, and in animal models, widespread coverage can be obtained by delivering the vector into the CSF.[81–84] The question has been where to enter the CSF for the maximal coverage. Investigations have targeted the larger reservoirs inside the brain (cerebral ventricles), outside the brain (cisterna magna), and into the thecal space in the spinal canal (subarachnoid space). Targeting the large cerebral ventricles (intraventricular route) in the frontal lobe of the brain is an easy surgical task, and is commonly used to deliver drugs to the CNS.[85–88] The advantages are that the slow pulsatile flow of the CSF allows movement of the vector around the brain without additional surgeries for effective coverage of the CNS.[89] The disadvantage is that the vector may be absorbed quickly into the chorionic villi and ependymal cells lining the ventricles.[82,85] Alternative less invasive routes of delivery of the gene therapy vector to the CSF include either delivery to the cisterna magna (intracisternal route) at the base of the skull or to the spinal canal subarachnoid space (intrathecal route). The intracisternal route has been shown by multiple studies in large animals to result in transgene expression throughout the CNS as effectively as the more invasive surgical intraventricular route, and involves a simple puncture to reach the CSF reservoir with minimal side effects.[90] Use of intrathecal delivery for gene therapy vectors has been limited to studies involving spinal cord and peripheral nerve disease.[90–93] The vectors stay predominantly in the lower spine in intrathecal delivery administrations. Of interest, vector distribution following intrathecal vector administration in NHPs was improved in one study if the animal was placed in the Trendelenburg tilted position during the intrathecal infusion, which led to superior expression in the brain, especially in the brain stem.[94] In contrast, a recent paper by Hinderer *et al*.[95] found that there was little impact of positioning the NHPs in this way following intrathecal administration. Finally, an additional non-surgical route—intranasal—has been tested delivering AAV9 via the nasal cavity in mice for mucopolysaccharidosis I, resulting in widespread detection of the transgene activity across the CNS.[96]

AAVrh.10-mediated delivery of APOE2

Based on the above considerations, three routes of AAV delivery of the *APOE2* gene to the CNS of NHPs (intraparenchymal, intraventricular, and intracisternal) were assessed in order to determine the optimal route of delivery that is both efficacious and safe. Vector administration included: (1) direct intraparenchymal administration to three sites in the hippocampal region (5×10^{12} gc total); (2) intracisternal (cisterna magna; 5×10^{13} gc); and (3) intraventricular (frontal horn of the third ventricle; 5×10^{13} gc). At 8 weeks post vector administration, the CNS was quantitatively evaluated for

APOE2 DNA, mRNA, and protein, and safety was evaluated by hematologic, serum chemistry, behavior, and MRI parameters. The data demonstrate that the direct hippocampal, intracisternal, and intraventricular routes all result in effective expression of ApoE2-HA in the hippocampal and entorhinal cortex region, the regions effected the earliest in AD,[39–42] and do so safely. Both the intracisternal and intraventricular routes result not only in intrahippocampal expression, but also in widespread expression throughout the brain. In the context that the intracisternal and intraventricular routes are equivalent in vector, APOE2 mRNA, and ApoE2-HA protein, and both routes are equally safe, it is concluded that since the intracisternal route is the least invasive, it is the choice as the best route for APOE2 gene therapy to treat *APOE4* homozygotes.

The widespread and safe transgene expression resulting from the relatively noninvasive intracisternal delivery is advantageous compared to the more localized delivery because in addition to the hippocampal region, other areas in the CNS are affected in AD.[20,43,44] Of interest, the connection to the entorhinal cortex, the olfactory bulb, is directly affected by changes in the perforant pathway, and one of the earliest pathological changes in AD.[43,49] Similarly, the loss of visual recognition is a characteristic pathology associated with AD.[50] Intracisternal delivery of AAVrh.10hAPOE2-HA vector resulted in ApoE2-HA detected by IHC in a wide range of substructures in the CNS, including the olfactory bulb and visual cortex, demonstrating that gene therapy with AAVrh.10hAPOE2 generates localized ApoE2 expression and secretion across width and breadth of the CNS, resulting in successful targeting the AD-associated regions.

Safety

General safety parameters, hematologic analysis, serum chemistry, and blinded videotape analysis of behavior parameters were assessed over the course of the study with all routes. The vector-administered groups did not differ from the sham control in any parameter. No adverse events or abnormal results were noted, suggesting that any of the three routes could be a viable method and route of delivery to target the regions of interest for the treatment of AD. Given that even minor trauma to the hippocampal region poses a significant risk, the direct intraparenchymal hippocampal route poses the greatest risk of an adverse event.[45–48] In that context, the less invasive intracisternal and intracerebroventricular routes of delivery were evaluated in NHPs at a dose scalable to humans. While the hippocampal region is important to short-term memory loss in AD and is the earliest region involved in the progression of the disease,[39–42] it is recognized that there would be advantages to having more widespread ApoE2 expression in the CNS, including: (1) while the early manifestations of the disease are in the hippocampal region, the amyloid deposition spreads, and the disease pathogenesis progressively involves a broad region of the brain; (2) ApoE2 is a secreted protein, and thus (assuming no toxicity) it should not matter where in the CNS it is produced, as long as it reaches the CSF, which circulates throughout the brain; and (3) based on the data in the present study in NHPs, therapeutic levels of ApoE2 in the CSF (>1 μg/mL) can be achieved with the least invasive intracisternal administration. In humans and rodents, ApoE levels in the CSF are 1–5 μg/mL.[97] If these levels of ApoE2 can be achieved in humans, this should be therapeutic, at a minimum converting an *APOE4* homozygote to an *E4/E2* heterozygote. From epidemiologic studies, this would markedly decrease the risk for developing early-onset AD compared to *E4* homozygotes.[6,12–14] Based on this rationale, intracisternal delivery in NHPs is safe and results in widespread expression of ApoE2, laying the framework for a clinical trial. In the recent study by Hinderer *et al.*,[95] comparison of intracisternal and intraventricular delivery of AAV9-GUSB (1.8×10^{13} gc, 1 mL) to mucopolysaccharidosis-afflicted canines found that the intraventricular route lead to inflammation and development of encephalitis. While no encephalitis was observed in any of the NHPs administered vector intraventricularly, this is a theoretical concern for the delivery route to the CSF.

It is recognized that any surgical procedure has risks, especially one involving the CNS, and it is proposed that clinical trials that administer gene therapy vectors via the intracisternal route use fluoroscopy to guide the placement of the catheter or spinal needle in the cisterna magna to avoid piercing of the cerebellum, medulla oblongata, or pons. To minimize the risk of the less commonly practiced intracisternal injection, placement of the spinal needle in the wider superior opening of the cisterna magna should be made via myelography, using a fluoroscope, to ensure correct placement without potential brainstem injury. Together, the risk/benefit ratio demonstrates that the intracisternal administration of AAVrh.10hAPOE2-HA leads to broad, widespread distribution of vector, transgene, and ApoE2 protein throughout the CNS, indicating that administration to the CSF via this route is sufficient and the least invasive.

ACKNOWLEDGMENTS

We thank Jojo Borja and Simon Morim for help with the CNS imaging studies, Veronica Mitchell for NHP behavior observations, and N. Mohamed for help with the manuscript. These studies were supported in part by the Alzheimer's Drug Discovery Foundation, # 20141209. The Center for Comparative Medicine and Pathology and the Laboratory of Comparative Pathology are supported in part by NCI Cancer Center Support Grant P30 CA008748. M.G.K was supported, in part, by the JPB Foundation.

AUTHOR DISCLOSURE

No competing financial interests exist.

REFERENCES

1. Hebert LE, Weuve J, Scherr PA, et al. Alzheimer disease in the United States (2010–2050) estimated using the 2010 census. Neurology 2013;80: 1778–1783.
2. Alzheimer's Assocation. 2017 Alzheimer's disease facts and figures. Alzheimers Dement 2017; 13:325–373.
3. Cummings JL, Morstorf T, Zhong K. Alzheimer's disease drug-development pipeline: few candidates, frequent failures. Alzheimers Res Ther 2014; 6:37.
4. Hung SY, Fu WM. Drug candidates in clinical trials for Alzheimer's disease. J Biomed Sci 2017;24:47.
5. Saunders AM, Strittmatter WJ, Schmechel D, et al. Association of apolipoprotein E allele epsilon 4 with late-onset familial and sporadic Alzheimer's disease. Neurology 1993;43:1467–1472.
6. Genin E, Hannequin D, Wallon D, et al. APOE and Alzheimer disease: a major gene with semidominant inheritance. Mol Psychiatry 2011;16: 903–907.
7. Mahley RW. Apolipoprotein E: remarkable protein sheds light on cardiovascular and neurological diseases. Clin Chem 2017;63:14–20.
8. Zannis VI, Breslow JL. Human very low density lipoprotein apolipoprotein E isoprotein polymorphism is explained by genetic variation and posttranslational modification. Biochemistry 1981; 20:1033–1041.
9. Corder EH, Saunders AM, Strittmatter WJ, et al. Gene dose of apolipoprotein E type 4 allele and the risk of Alzheimer's disease in late onset families. Science 1993;261:921–923.
10. Sando SB, Melquist S, Cannon A, et al. APOE epsilon 4 lowers age at onset and is a high risk factor for Alzheimer's disease; a case control study from central Norway. BMC Neurol 2008;8:9.
11. Farrer LA, Cupples LA, Haines JL, et al. Effects of age, sex, and ethnicity on the association between apolipoprotein E genotype and Alzheimer disease. A meta-analysis. APOE and Alzheimer Disease Meta Analysis Consortium. JAMA 1997; 278:1349–1356.
12. Conejero-Goldberg C, Gomar JJ, Bobes-Bascaran T, et al. APOE2 enhances neuroprotection against Alzheimer's disease through multiple molecular mechanisms. Mol Psychiatry 2014; 19:1243–1250.
13. Nagy Z, Esiri MM, Jobst KA, et al. Influence of the apolipoprotein E genotype on amyloid deposition and neurofibrillary tangle formation in Alzheimer's disease. Neuroscience 1995;69:757–761.
14. Corder EH, Saunders AM, Risch NJ, et al. Protective effect of apolipoprotein E type 2 allele for late onset Alzheimer disease. Nat Genet 1994;7: 180–184.
15. Liu CC, Liu CC, Kanekiyo T, et al. Apolipoprotein E and Alzheimer disease: risk, mechanisms and therapy. Nat Rev Neurol 2013;9:106–118.
16. Ellis RJ, Olichney JM, Thal LJ, et al. Cerebral amyloid angiopathy in the brains of patients with Alzheimer's disease: the CERAD experience, Part XV. Neurology 1996;46:1592–1596.
17. Kok E, Haikonen S, Luoto T, et al. Apolipoprotein E-dependent accumulation of Alzheimer disease-related lesions begins in middle age. Ann Neurol 2009;65:650–657.
18. Bales KR, Liu F, Wu S, et al. Human APOE isoform-dependent effects on brain beta-amyloid levels in PDAPP transgenic mice. J Neurosci 2009; 29:6771–6779.
19. Castellano JM, Kim J, Stewart FR, et al. Human apoE isoforms differentially regulate brain amyloid-beta peptide clearance. Sci Transl Med 2011;3: 89ra57.
20. Reiman EM, Chen K, Liu X, et al. Fibrillar amyloid-beta burden in cognitively normal people at 3 levels of genetic risk for Alzheimer's disease. Proc Natl Acad Sci U S A 2009;106:6820–6825.
21. Schmechel DE, Saunders AM, Strittmatter WJ, et al. Increased amyloid beta-peptide deposition in cerebral cortex as a consequence of apolipoprotein E genotype in late-onset Alzheimer disease. Proc Natl Acad Sci U S A 1993;90: 9649–9653.
22. Alves S, Fol R, Cartier N. Gene therapy strategies for Alzheimer's disease: an overview. Hum Gene Ther 2016;27:100–107.
23. Dodart JC, Marr RA, Koistinaho M, et al. Gene delivery of human apolipoprotein E alters brain Abeta burden in a mouse model of Alzheimer's disease. Proc Natl Acad Sci U S A 2005;102: 1211–1216.
24. Hudry E, Dashkoff J, Roe AD, et al. Gene transfer of human Apoe isoforms results in differential modulation of amyloid deposition and neurotoxicity in mouse brain. Sci Transl Med 2013;5: 212ra161.
25. Kaplitt M, Gouras GK, Makimura H, et al. Apolipoprotein E, A beta-amyloid, and the molecular pathology of Alzheimer's disease. Therapeutic implications. Ann New York Acad Sci 1996;802: 42–49.
26. Zhao L, Gottesdiener AJ, Parmar M, et al. Intracerebral adeno-associated virus gene delivery of apolipoprotein E2 markedly reduces brain amyloid pathology in Alzheimer's disease mouse models. Neurobiol Aging 2016;44:159–172.
27. Piguet F, Sondhi D, Piraud M, et al. Correction of brain oligodendrocytes by AAVrh.10 intracerebral gene therapy in metachromatic leukodystrophy mice. Hum Gene Ther 2012;23:903–914.
28. Sondhi D, Johnson L, Purpura K, et al. Long-term expression and safety of administration of AAVrh.10hCLN2 to the brain of rats and nonhuman primates for the treatment of late infantile neuronal ceroid lipofuscinosis. Hum Gene Ther Methods 2012;23:324–335.
29. Sondhi D, Peterson DA, Giannaris EL, et al. AAV2-mediated CLN2 gene transfer to rodent and nonhuman primate brain results in long-term TPP-I expression compatible with therapy for LINCL. Gene Ther 2005;12:1618–1632.
30. Rafi MA, Rao HZ, Luzi P, et al. Extended normal life after AAVrh10-mediated gene therapy in the mouse model of Krabbe disease. Mol Ther 2012; 20:2031–2042.
31. Rosenberg JB, Sondhi D, Rubin DG, et al. Comparative efficacy and safety of multiple routes of direct CNS administration of adeno-associated virus gene transfer vector serotype rh.10 expressing the human arylsulfatase A cDNA to nonhuman primates. Hum Gene Ther Clin Dev 2014;25:164–177.
32. Sondhi D, Hackett NR, Peterson DA, et al. Enhanced survival of the LINCL mouse following *CLN2* gene transfer using the rh.10 rhesus macaque-derived adeno-associated virus vector. Mol Ther 2007;15:481–491.
33. Sondhi D, Peterson DA, Edelstein AM, et al. Survival advantage of neonatal CNS gene transfer

for late infantile neuronal ceroid lipofuscinosis. Exp Neurol 2008;213:18–27.

34. Zerah M, Piguet F, Colle MA, et al. Intracerebral gene therapy using AAVrh.10-hARSA recombinant vector to treat patients with early-onset forms of metachromatic leukodystrophy: preclinical feasibility and safety assessments in nonhuman primates. Hum Gene Ther Clin Dev 2015;26:113–124.
35. Sondhi D, Rosenberg JB, De BP, et al. Long-term toxicology evaluation of AAVrh.10hARSA administration to the CNS of nonhuman primates to treat metachromatic leukodystrophy. Mol Ther 2016;24:S146.
36. De BP, Heguy A, Hackett NR, et al. High levels of persistent expression of alpha1-antitrypsin mediated by the nonhuman primate serotype rh.10 adeno-associated virus despite preexisting immunity to common human adeno-associated viruses. Mol Ther 2006;13:67–76.
37. Hackett NR, Redmond DE, Sondhi D, et al. Safety of direct administration of AAV2(CU)hCLN2, a candidate treatment for the central nervous system manifestations of late infantile neuronal ceroid lipofuscinosis, to the brain of rats and nonhuman primates. Hum Gene Ther 2005;16: 1484–1503.
38. Liddie S, Goody RJ, Valles R, et al. Clinical chemistry and hematology values in a Caribbean population of African green monkeys. J Med Primatol 2010;39:389–398.
39. Gomez-Isla T, Price JL, McKeel DW Jr, et al. Profound loss of layer II entorhinal cortex neurons occurs in very mild Alzheimer's disease. J Neurosci 1996;16:4491–4500.
40. Khan UA, Liu L, Provenzano FA, et al. Molecular drivers and cortical spread of lateral entorhinal cortex dysfunction in preclinical Alzheimer's disease. Nat Neurosci 2014;17:304–311.
41. Whitwell JL, Przybelski SA, Weigand SD, et al. 3D maps from multiple MRI illustrate changing atrophy patterns as subjects progress from mild cognitive impairment to Alzheimer's disease. Brain 2007;130:1777–1786.
42. Yang X, Yao C, Tian T, et al. A novel mechanism of memory loss in Alzheimer's disease mice via the degeneration of entorhinal-CA1 synapses. Mol Psychiatry 2018;23:199–210.
43. Lafaille-Magnan ME, Poirier J, Etienne P, et al. Odor identification as a biomarker of preclinical AD in older adults at risk. Neurology 2017;89: 327–335.
44. Tang X, Qin Y, Wu J, et al. Shape and diffusion tensor imaging based integrative analysis of the hippocampus and the amygdala in Alzheimer's disease. Magn Reson Imaging 2016;34:1087–1099.
45. Davies KG, Bell BD, Bush AJ, et al. Naming decline after left anterior temporal lobectomy correlates with pathological status of resected hippocampus. Epilepsia 1998;39:407–419.
46. Hampton RR, Buckmaster CA, Anuszkiewicz-Lundgren D, et al. Method for making selective lesions of the hippocampus in macaque monkeys using NMDA and a longitudinal surgical approach. Hippocampus 2004;14:9–18.
47. Horel JA. The neuroanatomy of amnesia. A critique of the hippocampal memory hypothesis. Brain 1978;101:403–445.
48. Rydenhag B, Silander HC. Complications of epilepsy surgery after 654 procedures in Sweden, September 1990–1995: a multicenter study based on the Swedish National Epilepsy Surgery Register. Neurosurgery 2001;49:51–56; discussion 56–57.
49. Daulatzai MA. Olfactory dysfunction: its early temporal relationship and neural correlates in the pathogenesis of Alzheimer's disease. J Neural Transm (Vienna) 2015;122:1475–1497.
50. Tzekov R, Mullan M. Vision function abnormalities in Alzheimer disease. Surv Ophthalmol 2014; 59:414–433.
51. Woodward RA, Weld KP. A comparison of ketamine, ketamine-acepromazine, and tiletamine-zolazepam on various hematologic parameters in rhesus monkeys (*Macaca mulatta*). Contemp Top Lab Anim Sci 1997;36:55–57.
52. Choudhury SR, Hudry E, Maguire CA, et al. Viral vectors for therapy of neurologic diseases. Neuropharmacology 2017;120:63–80.
53. Joshi CR, Labhasetwar V, Ghorpade A. Destination brain: the past, present, and future of therapeutic gene delivery. J Neuroimmune Pharmacol 2017;12:51–83.
54. Wild EJ, Tabrizi SJ. Therapies targeting DNA and RNA in Huntington's disease. Lancet Neurol 2017; 16:837–847.
55. Herzog CD, Bishop KM, Brown L, et al. Gene transfer provides a practical means for safe, long-term, targeted delivery of biologically active neurotrophic factor proteins for neurodegenerative diseases. Drug Deliv Transl Res 2011;1:361–382.
56. Hocquemiller M, Giersch L, Audrain M, et al. Adeno-associated virus-based gene therapy for CNS diseases. Hum Gene Ther 2016;27:478–496.
57. Janson C, McPhee S, Bilaniuk L, et al. Clinical protocol. Gene therapy of Canavan disease: AAV-2 vector for neurosurgical delivery of aspartoacylase gene (ASPA) to the human brain. Hum Gene Ther 2002;13:1391–1412.
58. Lau AA, Hemsley KM. Adeno-associated viral gene therapy for mucopolysaccharidoses exhibiting neurodegeneration. J Mol Med (Berl) 2017;95: 1043–1052.
59. Leone P, Shera D, McPhee SW, et al. Long-term follow-up after gene therapy for canavan disease. Sci Transl Med 2012;4:165ra163.
60. Sevin C, Aubourg P, Cartier N. Enzyme, cell and gene-based therapies for metachromatic leukodystrophy. J Inherit Metab Dis 2007;30:175–183.
61. Smith BK, Collins SW, Conlon TJ, et al. Phase I/II trial of adeno-associated virus-mediated alpha-glucosidase gene therapy to the diaphragm for chronic respiratory failure in Pompe disease: initial safety and ventilatory outcomes. Hum Gene Ther 2013;24:630–640.
62. Tardieu M, Zerah M, Husson B, et al. Intracerebral administration of adeno-associated viral vector serotype rh.10 carrying human SGSH and SUMF1 cDNAs in children with mucopolysaccharidosis type IIIA disease: results of a Phase I/II trial. Hum Gene Ther 2014;25:506–516.
63. Wirth B, Barkats M, Martinat C, et al. Moving towards treatments for spinal muscular atrophy: hopes and limits. Expert Opin Emerg Drugs 2015; 20:353–356.
64. Worgall S, Sondhi D, Hackett NR, et al. Treatment of late infantile neuronal ceroid lipofuscinosis by CNS administration of a serotype 2 adeno-associated virus expressing CLN2 cDNA. Hum Gene Ther 2008;19:463–474.
65. Bonnemann CG, Bharucha-Goebel DX, Gray SJ. Giant axonal neuropathy: natural history, outcome measures, and intrathecal AAV9 mediated gene transfer. Neuromuscul Disord 2017;27S1:S2.
66. Golebiowski D, Bradbury AM, Kwon C-S, et al. AAV gene therapy strategies for lysosomal storage disorders with central nervous system involvement. In: Bo X, Verhaagen J, eds. Gene Delivery and Therapy for Neurological Disorders, Neuromethods. New York: Springer Science+Business Media, 2015:265–295.
67. Grieger JC, Samulski RJ. Packaging capacity of adeno-associated virus serotypes: impact of larger genomes on infectivity and postentry steps. J Virol 2005;79:9933–9944.
68. Cearley CN, Vandenberghe LH, Parente MK, et al. Expanded repertoire of AAV vector serotypes mediate unique patterns of transduction in mouse brain. Mol Ther 2008;16:1710–1718.
69. Aschauer DF, Kreuz S, Rumpel S. Analysis of transduction efficiency, tropism and axonal transport of AAV serotypes 1, 2, 5, 6, 8 and 9 in the mouse brain. PLoS One 2013;8:e76310.
70. Liu G, Martins IH, Chiorini JA, et al. Adeno-associated virus type 4 (AAV4) targets ependyma and astrocytes in the subventricular zone and RMS. Gene Ther 2005;12:1503–1508.
71. Rosenberg JB, Kaminsky SM, Aubourg P, et al. Gene therapy for metachromatic leukodystrophy. J Neurosci Res 2016;94:1169–1179.
72. Thwaite R, Pages G, Chillon M, et al. AAVrh.10 immunogenicity in mice and humans. Relevance of antibody cross-reactivity in human gene therapy. Gene Ther 2015;22:196–201.
73. Tardieu M, Zerah M, Gougeon ML, et al. Intracerebral gene therapy in children with mucopolysaccharidosis type IIIB syndrome: an uncontrolled Phase 1/2 clinical trial. Lancet Neurol 2017;16: 712–720.
74. Kaplitt MG, Feigin A, Tang C, et al. Safety and tolerability of gene therapy with an adeno-associated virus (AAV) borne GAD gene for Parkinson's disease: an open label, Phase I trial. Lancet 2007;369:2097–2105.

75. Aubourg P. Gene therapy for leukodystrophy: progress, challenges and opportunities. Expert Opin Orphan Drugs 2016;4:359–367.

76. Souweidane MM, Fraser JF, Arkin LM, et al. Gene therapy for late infantile neuronal ceroid lipofuscinosis: neurosurgical considerations. J Neurosurg Pediatr 2010;6:115–122.

77. Colle MA, Piguet F, Bertrand L, et al. Efficient intracerebral delivery of AAV5 vector encoding human ARSA in non-human primate. Hum Mol Genet 2010;19:147–158.

78. Hadaczek P, Forsayeth J, Mirek H, et al. Transduction of nonhuman primate brain with adeno-associated virus serotype 1: vector trafficking and immune response. Hum Gene Ther 2009;20:225–237.

79. Rosenbluth KH, Eschermann JF, Mittermeyer G, et al. Analysis of a simulation algorithm for direct brain drug delivery. NeuroImage 2012;59:2423–2429.

80. Varenika V, Kells AP, Valles F, et al. Controlled dissemination of AAV vectors in the primate brain. Prog Brain Res 2009;175:163–172.

81. Bucher T, Dubreil L, Colle MA, et al. Intracisternal delivery of AAV9 results in oligodendrocyte and motor neuron transduction in the whole central nervous system of cats. Gene Ther 2014;21:522–528.

82. Davidson BL, Stein CS, Heth JA, et al. Recombinant adeno-associated virus type 2, 4, and 5 vectors: transduction of variant cell types and regions in the mammalian central nervous system. Proc Natl Acad Sci U S A 2000;97:3428–3432.

83. Gray SJ, Nagabhushan Kalburgi S, McCown TJ, et al. Global CNS gene delivery and evasion of anti-AAV-neutralizing antibodies by intrathecal AAV administration in non-human primates. Gene Ther 2013;20:450–459.

84. Samaranch L, Salegio EA, San Sebastian W, et al. Adeno-associated virus serotype 9 transduction in the central nervous system of nonhuman primates. Hum Gene Ther 2012;23:382–389.

85. Herenu CB, Sonntag WE, Morel GR, et al. The ependymal route for insulin-like growth factor-1 gene therapy in the brain. Neuroscience 2009;163:442–447.

86. Pardridge WM. CSF, blood–brain barrier, and brain drug delivery. Expert Opin Drug Deliv 2016; 13:963–975.

87. Regev L, Ezrielev E, Gershon E, et al. Genetic approach for intracerebroventricular delivery. Proc Natl Acad Sci U S A 2010;107:4424–4429.

88. Katz ML, Coates JR, Sibigtroth CM, et al. Enzyme replacement therapy attenuates disease progression in a canine model of late-infantile neuronal ceroid lipofuscinosis (CLN2 disease). J Neurosci Res 2014;92:1591–1598.

89. Katz ML, Tecedor L, Chen Y, et al. AAV gene transfer delays disease onset in a TPP1-deficient canine model of the late infantile form of Batten disease. Sci Transl Med 2015;7:313ra180.

90. Pleticha J, Heilmann LF, Evans CH, et al. Preclinical toxicity evaluation of AAV for pain: evidence from human AAV studies and from the pharmacology of analgesic drugs. Mol Pain 2014;10:54.

91. Beutler AS. AAV provides an alternative for gene therapy of the peripheral sensory nervous system. Mol Ther 2010;18:670–673.

92. Bevan AK, Duque S, Foust KD, et al. Systemic gene delivery in large species for targeting spinal cord, brain, and peripheral tissues for pediatric disorders. Mol Ther 2011;19:1971–1980.

93. Towne C, Schneider BL, Kieran D, et al. Efficient transduction of non-human primate motor neurons after intramuscular delivery of recombinant AAV serotype 6. Gene Ther 2010;17:141–146.

94. Meyer K, Ferraiuolo L, Schmelzer L, et al. Improving single injection CSF delivery of AAV9-mediated gene therapy for SMA: a dose–response study in mice and nonhuman primates. Mol Ther 2015;23:477–487.

95. Hinderer C, Bell P, Katz N, et al. Evaluation of intrathecal routes of administration for adeno-associated viral vectors in large animals. Hum Gene Ther 2018;29:15–24.

96. Belur LR, Temme A, Podetz-Pedersen KM, et al. Intranasal adeno-associated virus mediated gene delivery and expression of human iduronidase in the central nervous system: a noninvasive and effective approach for prevention of neurologic disease in mucopolysaccharidosis type I. Hum Gene Ther 2017;28:576–587.

97. Koch S, Donarski N, Goetze K, et al. Characterization of four lipoprotein classes in human cerebrospinal fluid. J Lipid Res 2001;42: 1143–1151.

Received for publication November 17, 2017;
accepted after revision January 27 2018.

Published online: February 6, 2018.